1918
TALLINNA
TEHNIKAÜLIKOOL

INFOTEHNOLOOGIA-
TEADUSKOND

Rauno Gordon

Modelling of Cardiac Dynamics and Intracardiac Bioimpedance

DOCTOR OF PHILOSOPHY THESIS

Supervisors:	Prof. Mart Min Dr. Toomas Parve
Reviewers:	Prof. Kalju Meigas Dr. Rodney Salo
Opponents:	Prof. Jari Hyttinen Dr. Jüri Vedru

Faculty of Information Technology
Department of Electronics
TALLINN UNIVERSITY OF TECHNOLOGY

Dissertation was accepted for defence of degree of Doctor of Philosophy in Engineering Sciences on January 3, 2007.

Supervisors:	Prof. Mart Min	Faculty of Information Technology, Tallinn University of Technology, Estonia
	Dr. Toomas Parve	Faculty of Information Technology, Tallinn University of Technology, Estonia
Reviewers:	Prof. Kalju Meigas	Biomedical Engineering Centre, Tallinn University of Technology, Estonia
	Dr. Rodney Salo	Basic Research Department, Boston Scientific, USA
Opponents:	Prof. Jari Hyttinen	Ragnar Granit Institute, Tampere University of Technology, Finland
	Dr. Jüri Vedru	Institute of Experimental Physics and Technology, the University of Tartu, Estonia

Oral defence: 9.3.2007, 14.00, Tallinn, Ehitajate tee 5, room VII-226.

Declaration

Hereby I declare that this doctoral thesis, my original investigation and achievement, submitted for the doctoral degree at Tallinn University of Technology has not been submitted before for any degree or examination.

Rauno Gordon

Copyright Rauno Gordon, 2007
ISSN: 1406-4731
ISBN: 978-9985-59-691-3

1918
TALLINNA
TEHNIKAÜLIKOOL

INFOTEHNOLOOGIA-
TEADUSKOND

Rauno Gordon

Südame dünaamika ja südamesisese bioimpedantsi modelleerimine

VÄITEKIRI

Juhendajad:	Prof. Mart Min Dr. Toomas Parve
Hindajad:	Prof. Kalju Meigas Dr. Rodney Salo
Oponendid:	Prof. Jari Hyttinen Dr. Jüri Vedru

Abstract

This thesis describes a system for studying the relation between cardiac stroke volume and intracardiac bioimpedance signal. The system is a MATLAB based software composed of 3D dynamic heart modelling part and simulation part for bioimpedance signal computation. This system allows to conduct virtual experiments with heart models that can be designed based on characteristics of real dynamic hearts. These characteristics include size and shape of the whole heart and compartments, various properties of dynamics like duration and timing of systole and diastole, speed and precise timeline of contraction of compartments, and the frequency dependent electrical impedivities of tissues present in the modelling domain (lung, muscle and blood). The simulation part of the system carries out bioimpedance signal computation with Finite Difference Method (FDM). Electrode locations and current can be specified in the virtual heart and the FDM computes the complex values of electrical potential at discrete locations in the whole modelling domain. This method effectively gives the solution to the forward problem of electrical bioimpedance.

Sample results of the working system are presented as simulated complex impedance signals at the catheter electrodes with 5 different stroke volumes of the heart and at 2 different frequencies. The simulation results show that magnitude and also phase of the impedance signal correlates with the changing volume of the heart.

The simulated impedance signals are also compared with the results of simple equivalent circuit models. The comparison shows that simple equivalent circuit models exhibit similar behavior as FDM simulation and with careful selection of parameters simple models could substitute computation-intensive modelling in some practical cases.

The impedance of static heart at a wide frequency range is calculated to study the performance of FDM with anisotropic tissue impedances. This study clearly presented the problem-areas of the FDM mesh and indicated the extent of errors that improper use of anisotropy could introduce.

Sample results of the whole electric field are presented as consisting of real-imaginary components and alternatively of magnitude-phase components. It is concluded that visualization of the whole electric field in the simulation of bioimpedance measurement can be used to better understand the behavior of the signals.

The results suggest that FDM simulation gives usable results in bioimpedance forward problem computation. Before results of virtual experiments on dynamic heart models can be compared to results of real experiments on real hearts, modelling techniques have to evolve. The accuracy of the heart model is to be increased and larger area of the chest has to be included. A fast method of creating a model of a particular heart has to be developed before virtual experimentation can replace real experiments.

Kokkuvõte

Südame dünaamika ja südamesisese bioimpedantsi modelleerimine

See dissertatsioon kirjeldab tarkvaralist süsteemi, mis võimaldab uurida südame löögimahu ja südamesisese bioimpedantsi vahelise seost. Tarkvaraline süsteem põhineb MATLAB'il ning koosneb kahest osast. Üks osa võimaldab modelleerida kolme-mõõtmelist ja liikuvat südant ning teine osa simuleerida bioimpedantsi signaale. Süsteem võimaldab seega teostada virtuaalseid katseid südame mudelitega, mis on koostatud vastavalt reaalsete dünaamiliste südamete parameetritele. Nendeks parameetriteks on südame ja tema kambrite suurus ja kuju, erinevad dünaamika omadused, nagu süstoli ja diastoli algus ning kestus, kambrite kontraktsiooni täpne kiirus ja kulg ning südame kudede (veri, lihas ja kops) sagedussõltuvad erijuhtivused. Bioimpedantsi simuleeriv osa arvutab potentsiaalide jaotumist südame mudelis FDM-meetodiga (Finite Difference Method). Virtuaalses südames saab määrata elektroodide asukohad ning neid läbiva voolu. Seejärel arvutatakse FDM-meetodiga kompleks-arvulise potentsiaali väärtused diskreetse jaotusega punktides üle kogu modelleeritava piirkonna.

Näidisena on töötava süsteemi tulemused esitatud südame-kateetri elektroodide impedantsi-signaalidena. Signaalid simuleeriti viiel erineva löögimahuga südame mudelil kahel mõõtesagedusel. Tulemused näitasid, et impedantsi signaali suurus ja ka faas korreleeruvad südame muutuva mahuga.

Simuleeritud impedantsi signaale võrreldi ka lihtsate elektriliste aseskeemide tulemustega. Võrdlusest oli näha, et lihtsad elektrilised aseskeemid käituvad sarnaselt FDM simulatsioonile ning hoolika parameetrite valikuga võiksid lihtsad elektrilised aseskeemid mõnel praktilisel juhul asendada arvutusmahukaid simuleerimise meetodeid.

Uurimistöö käigus uuriti ka FDM-meetodi käitumist anisotroopsete kudede omaduste korral. Selleks simuleeriti impedantsi signaali jaotumist staatilises südames laias sagedus-vahemikus. See uurimus näitas väga selgelt FDM-võrgu probleemseid kohti ning viitas arvutuslikele vigadele, mida anisotroopsuse kasutamine võib tekitada.

Impedantsi simulatsiooni näidistulemused on esitatud ka terve kolme-mõõtmelise elektriväljana, mis koosneb reaal- ja imaginaar komponentidest. Alternatiivina on toodud ka amplituudi ja faasina kujutatud tulemused. Uurides neid tulemusi on järeldatud, et kogu elektri-välja kujutamine bioimpedantsi mõõtmise

simulatsioonis aitab signaalide käitumist paremini mõista.

Uurimuste tulemused näitavad, et FDM-simulatsioon annab täiesti kasutatavaid tulemusi bioimpedantsi otse-probleemi arvutamisel. Enne, kui dünaamilistel südamemudelitel tehtud virtuaalsete eksperimentide tulemusi saaks võrrelda tõelistel südametel mõõdetud reaalsete tulemustega, peavad modelleerimise võimalused arenema. Parandama peab südame mudeli täpsust ning mudelisse peab kaasama suuremat osa rindkerest. Enne peab arendama välja reaalse südame modelleerimise kiire meetodi, kui virtuaalsed katsed saaksid asendada reaalseid katseid.

Acknowledgements

I have been studying and working on this thesis about four and a half years by now, but my venture into the world of bioimpedance started two years before that. During all this time I have had my supervisor Prof. Mart Min to guide me through the numerous different subjects involved. Thank You very much, Mart, for having faith in me all this time.

I would also like to thank Dr. Toomas Parve, my second supervisor, for all the scientific and philosophical discussions.

I need to thank our medical people Andres Kink and Indrek Rätsep, who showed me real blood and explained details about the heart.

For the biggest impact to my scientific work I am very grateful to the team in Tampere University of Technology, Ragnar Granit Institute. I had the opportunity to spend two winters there and those were the most fruitful periods during my PhD studies. Specifically I am grateful to Prof. Jaakko Malmivuo, the head of the institute, for accepting me there generously and sharing his wisdom and vision.

My sincere thanks also to Tuukka Arola, Katrina Wendel and Outi Ryynanen whom I met in Tampere. A big part of my work was accomplished with their support. I am glad they survived my harassment and participated with enthusiasm. I am hoping to continue working with you.

I also owe thanks to the team in Physics Department of the University of Tartu. I am happy I had the chance to work with Sergei Maltchenko and Konstantin Skaburskas. They had an impact on my scientific results and I hope our cooperation continues.

An essential impact to my work and future perspectives has been given by the Basic Research Department of Guidant Corporation (USA), through both, financial support in frames of the Collaborating Agreement with our University, and practical advices of Dr. Rodney W. Salo. I sincerely hope to continue the work in touch with him.

All this time I felt the support from my home organization - Department of Electronics at Tallinn University of Technology.

I am truly grateful to my mother and father who gave me my genes and lifeforce.

Many thanks also to my friends in my martial arts class, who gave me bruises when I needed them.

List of publications

R. Gordon, A. Kuusik. Bio-Impedance FDM-Modeling Inside Heart for Application in Implanted Devices. Electrocardiology 2004 (778 - 782). Singapore: World Scientific Publishing Co. 2005.

R. Gordon, R. Land, M. Min, T. Parve, R. Salo. A Virtual System for Simultaneous Multifrequency Measurement of Electrical Bioimpedance. International Journal of Bioelectromagnetism, vol.7(2), 243 - 246. 2005.

R. Gordon. Simulation of Intra-Cardiac Complex Impedance Signals for Developing Simple Bio-Impedance Models for Cardio-Dynamics. In: Proceedings of the 10th Biennial International Baltic Electronics Conference: 2006 International Baltic Electronics Conference (BEC 2006), 2-4 October 2006, Tallinn-Laulasmaa, Estonia. Tallinn, Estonia: IEEE Operations Center, 2006, 213 - 216. 2006.

R. Gordon, T. Arola, K. Wendel, O. Ryynänen, J. Hyttinen. Accuracy of numerical methods in solving static and quasistatic electric fields. M. Min (Toim.). Proc. of the Estonian Academy of Sciences. Special issue on Electronics. Tallinn: Estonian Academy Publishers, 262 - 283. 2006.

R. Gordon. Simulation of Intra-Cardiac Catheter Complex Impedance Signals with Variable Stroke Volume. In: Proceedings of the 28th Annual International Conference of the IEEE Engineering in Medicine and Biology Society: 28th Annual International Conference of the IEEE Engineering in Medicine and Biology Society, New York City, New York, USA, 30.08 - 3.09, 2006. New York, USA: IEEE, 2006, 2892 - 2895. 2006.

R. Gordon, S. Malchenko, I. Rätsep. Modeling the Dynamic Heart for Impedance Based Cardiac Pathology Detection. In: IFBME Proceedings 2005: 3rd European Medical & Biological Engineering Conference; IFMBE European Conference on Biomedical Engineering EMBEC'05, Prague, Czech Republic, November 20-25, 2005. IFMBE, 2005, (11), 2146 - 2149. 2005.

R. Gordon, A. Haapalainen, P. Kauppinen, R. Land. Bioimpedance Analysis

of Cardiac Function Using In-Vivo Experiments, Measurement and Simulation. In: Proc of the 13th Nordic Baltic Conference on Biomedical Engineering and Medical Physics (NBC'05 UME),: 13th Nordic Baltic Conference on Biomedical Engineering and Medical Physics, June 13-17, 2005, Ume, Sweden. Ume, Sweden: IFMBE, 2005, 309 - 310. 2005.

R. Gordon. Organ Bio-Impedance Modelling with 3D Mesh of Equivalent Cirquits. Proceedings of the XII International Conference on Electrical Bio-Impedance (ICEBI 04). Gdansk, Poland, 2004, ISBN 83-917681-6-3, 715-718. 2004.

R. Gordon. Heart Bioimpedance 3D FDM Modelling with Anisotropic Tissue Properties. In: Proceedings of the 9th Biennial Baltic Electronics Conference (BEC 2004). Tallinn, Estonia, 2004, ISBN 9985-59-462-2, 175-178. 2004.

R. Gordon, A. Kuhlberg, M. Min, T. Parve. Sensing of Physiological Dynamic Processes using Measurement of Electrical Bioimpedance. In: Proceedings of SENSORS and SYSTEMS International Conference June 24-27, 2002 Saint-Petersburg, RUSSIA. 2002.

R. Gordon, T. Parve. Electrical Bioimpedance Measurement: methods and equivalent circuits. In: Proceedings of the 8th Biennial Baltic Electronics Conference BEC2002 October 6-9, 2002 Tallinn, ESTONIA. 2002.

R. Gordon. Heartwork Analysis using Bioimpedance Method. In: Telekommunikatsioon 2002, Rahvusvahelise Telekommunikatsioonipäeva konverentsi materjalid, Tallinn. 6 pages. 2002.

R. Gordon. Südame energiabilansi möötmine. In: Rahvusvahelise Telekommunikatsioonipäeva konverents 18. mai 2001 (http://www.elin.ttu.ee/EEU-Elec/KonvWrks/EWSH01/CardioEn/). 2001.

Table of Contents

Abstract i
Kokkuvõte iii
Acknowledgements v
List of publications vi
List of Figures xi

1 Introduction **1**
1.1 Importance of the study 1
1.1.1 Heart function 1
1.1.2 Vasculatory system 1
1.1.3 Modelling 2
1.2 Aims of the work 2

2 Background **3**
2.1 Electrical bioimpedance 3
2.2 Electrolytes 3
2.3 Bioimpedance measurement 4
2.4 Measurement instrumentation 5
2.5 Implanted measurement devices 5
2.6 Contact problem 6
2.7 Measured tissue impedances 7
2.8 Equivalent circuit models 8
2.9 Electro-quasistatic problem, complex numbers 11
2.10 Laplace's equation, Poisson's equation 11
2.11 Numerical solution, FDM 12
2.12 Forward problem 13
2.13 Heart anatomy 14

2.14 Myocardial fibre structure 15
2.15 Anatomy dynamics 16

3 Materials and methods 18
3.1 Modelling and simulation pipeline description 18
3.2 Static 3D spline model creation 19
3.3 Animating the geometry 21
3.4 Tissue modelling method and actual models used 33
3.5 FDM matrix generation 36
3.6 Solving the matrix equation 37

4 Results 39
4.1 Overview of published and presented work 39
4.1.1 Study nr. 1: Simulation of Intra-Cardiac Catheter Complex Impedance Signals with Variable Stroke Volume . . . 39
4.1.2 Study nr. 2: Simulation of Intra-Cardiac Complex Impedance Signals for Developing Simple Bio-impedance Models for Cardio-Dynamics 41
4.1.3 Study nr. 3: Bio-Impedance FDM-Modelling Inside Heart for Application in Implanted Devices 41
4.1.4 Study nr. 4: A Virtual System for Simultaneous Multi-frequency Measurement of Electrical Bioimpedance . . . 42
4.1.5 Study nr. 5: Accuracy of numerical methods in solving static and quasistatic electric fields 43
4.2 Discussion 44
4.3 Future studies 46
4.4 Conclusions 47

Bibliography 49

5 Appendixes 54
Appendix I: Curriculum Vitae 54
Appendix II: MATLAB features and capabilities 58
Appendix III: Simulation of Intra-Cardiac Catheter Complex Impedance Signals with Variable Stroke Volume 63

Appendix IV: Simulation of Intra-Cardiac Complex Impedance Signals for Developing Simple Bio-impedance Models for Cardio-Dynamics 69
Appendix V: Bio-Impedance FDM-Modelling Inside Heart for Application in Implanted Devices 75
Appendix VI: A Virtual System for Simultaneous Multi-frequency Measurement of Electrical Bioimpedance 81
Appendix VII: Accuracy of numerical methods in solving static and quasistatic electric fields 87

List of Figures

2.1 Frequency dependence of dielectric permittivity and admittivity of muscle tissue. 9
2.2 Basic principle of a tissue electric equivalent. 10
2.3 Cross-section of the heart during end-diastole and end-systole. . . 15
2.4 Myocardial fibre structure. 16
2.5 Dynamics of left ventricle volume and pressure. 17

3.1 Compartments of the spline heart model. 20
3.2 The dynamic heart modelling system with a sample heart model file (”splart1_splines4D-33_newNY2.mat”) loaded and shown in the main dialog window (”splart1”). 22
3.3 Components of spherical coordinates. 24
3.4 The static spline editing toolset. Can also be applied to dynamic compartments. 25
3.5 The spline dynamics editing toolset. 27
3.6 The graphic equalizer window with an image from a textbook [Schmidt and Thews (1990)] loaded to the background for help. . 29
3.7 Smoothing tool. 30
3.8 Volume estimation and volume data exporting toolset. 32
3.9 Bode plot of the three tissues used in bioimpedance simulation. . . 34

4.1 Intra-cardiac bioimpedance simulation results shown as current flow-tubes (left) and iso-surfaces of phase angle distribution (right). The heart is viewed from the back, catheter with electrodes is inserted to the left ventricle and the current goes from one electrode to another inside the left ventricle. 45

Chapter 1

Introduction

1.1 Importance of the study

1.1.1 Heart function

The pumping function of the heart is hard to classify reliably. Heart has traditionally been described as a positive displacement pump. It has also been described as a dynamic displacement pump [Lundbäck (1986)]. Remarkably the heart is able to maintain the stroke volume and energy-efficiency over such a wide range of beating rates. It has been observed, that when the chest is opened during open-heart surgery, the performance of the heart changes drastically [Hoit et al. (1997)]. The Heart also has an ability to work in a wide spectrum of system load, muscle conditions and body positions. During all these conditions and working modes the heart maintains the balance of the left and right side stroke volume although the pressures, total chamber volumes and energy consumption of the two sides are vastly different. This flexibility and adaptiveness of the heart is beyond our current comprehension and makes the modelling of the heart function a difficult challenge. When considering the inter-patient variability of heart shapes, the modelling task seems downright daunting.

1.1.2 Vasculatory system

The vasculatory system of the human body needs a constant flow to carry out its tasks for the organism and also to sustain itself. The heart is the principal engine behind the bloodflow in the vasculatory system. Bloodflow is maintained with constant pressure difference between aorta (source) and systemic veins (sink).

The heart has two sides with different pressure and work loads. The right side of the heart pumps blood from systemic veins of low pressure to pulmonary arteries of higher pressure [Vander et al. (1990a)]. This blood goes through the lungs, where blood is oxygenated and excess CO is released. The oxygen-rich blood then enters the left side of the heart through pulmonary veins. The left heart then does its' work again to raise the pressure and pumps the blood into the aorta [Vander et al. (1990a)].

1.1.3 Modelling

Cardiac dynamics modelling, the way it has been designed here, has relevance in diagnose and possible healthcare in various pathologic conditions of the heart and vasculatory system.

The heart modelling system presented in this thesis has primarily been developed for intracardiac bioimpedance measurement simulation. One of the goals of research in intracardiac bioimpedance is cardiac stroke volume estimation. Stroke volume information can be used directly by cardiac pacemakers that strive to set the pacing rate adaptively. In a chronotropically insufficient heart the natural heart rate will not increase with the increase of the body demand, but there will be an increase in the contractility of the heart. Measuring the contractility (stroke volume) will give us indication of the desired pacing rate [Webster (1995)]. Impedance measurement has the added benefit of monitoring myocardium health in medical practice.

1.2 Aims of the work

- To develop a computer-modelling system capable of designing the heart with different stroke volumes.
- To create a heart model that is geometrically modifiable.
- To conduct virtual experiments: simulate impedance measurement scenarios inside the heart.

Chapter 2

Background

2.1 Electrical bioimpedance

Electrical bioimpedance is the study of passive electrical properties of biologic objects and tissues. If we apply voltage to a biological study object and measure the passing current, we are essentially dealing with bioimpedance [Grimnes and Martinsen (2000)]. This can also be done the other way around, introducing current and measuring voltage drop. If on the other hand, we are not measuring the current or voltage and our aim is to make changes in the object with electricity, then we are not dealing with bioimpedance, but rather with electrotherapy or electrocution. In a more general case, where there are endogenic electric sources in the object or the measurement is changing the object, we are dealing with bioelectricity [Grimnes and Martinsen (2000)]. From electrical point-of-view immitance is the combined term of impedance and admittance. Bioimmitance would therefore be more correct in the title of the thesis although bioimpedance is more widely used and will gain general recognition.

Charge carriers inside biologic objects are mostly ions. Living tissue is therefore predominantly an electrolytic conductor [Grimnes and Martinsen (2000)].

2.2 Electrolytes

Living tissue contains ions that are free to migrate in the intracellular and extracellular media. There is rarely a separate flow of electrons in living tissue. In living tissue electronic current is only found in DNA molecules inside the cells [Grimnes

and Martinsen (2000)]. The current flowing inside living tissue therefore is mostly a current of ions and that means transport of substance. If the current applied is a DC current, it can not last for a long time without changing the conductor (tissue).

2.3 Bioimpedance measurement

Bioimpedance is usually measured with alternating current to lessen the ion-transport effect in the tissue. The term ”impedance” is also used for frequency dependent measurement, otherwise we would be measuring resistance. Inside the electrodes (metals) the charge carriers are electrons, inside the tissue however, charge is carried by ions as previously noted. Current passing from an electrode into a tissue must change the charge carriers on the material boundary. With DC current and low frequencies there are several effects at the material boundary, like discharging, diffusion and decomposition of molecules. These effects depend on the particular ions present, electrode materials and current. The actual effects at work on the boundary are outside the scope of this thesis. This thesis is about high frequency (1 kHz and above) bioimpedance simulation and at those high frequencies we do not have to deal with the ionic-electronic conduction issue. If the excitation is sinusoidal and the measured AC voltage (or current) is also sinusoidal, then we have a linear response (the whole system, electrodes and tissue, is responding linearly). In 1982 Onaral and Schwan measured impedance dependence of frequency and potential with platinum electrodes in saline solution [Onaral and Schwan (1982), Schwan (1963)]. They found a frequency-independent voltage amplitude limit for linear behavior. The average limit was about 100mV AC. The corresponding current limit at the same time was frequency dependent: 5 μA/cm2 in the millihertz range, 100 mA/cm2 in the higher kilohertz range. Here, in this thesis the actual electrode material is not specified. The frequencies used are high enough and the current low enough to be safely inside the limits of linearity.

To minimize the ion-transport effect in the tissue, the measurement AC current must also be polarity-balanced and alternation with single-polarity amplitude change is often not enough [Grimnes and Martinsen (2000)].

2.4 Measurement instrumentation

Historically bridges have been used for bioimpedance measurement [Schwan (1963), Schwan and Ferris (1968), Hayakawa et al. (1975)]. Today however they have given way to lock-in amplifiers and impedance analyzers. Digital lock-in amplifiers are based on the multiplication of two sine waves. One wave carries the amplitude (and phase) -modulated signal and the other is a reference with the chosen amplitude and phase [Grimnes and Martinsen (2000)]. Some lock-in amplifiers also enable harmonic analysis by using additional reference signals with frequencies equal to multiples of the base frequency. Digital lock-in amplifiers have a very wide frequency range, starting from the μHz and going up to the GHz range. The upper frequency limit is defined by the analog-digital converter [Vistnes et al. (1984)].

Analog lock-in amplifiers are basically synchronous rectifiers, that contain a phase sensitive detector and a low-pass filter. In the phase sensitive detector multiplies two signals, the measured input and a reference. The reference signal controls a switch and therefore behaves as a square wave. The synchronous rectifier is sensitive to the reference frequency, but also to all the Fourier components (the odd harmonic components) of the frequency [Grimnes and Martinsen (2000), Meade (1989), Min and Parve (1996b)].

Some analog lock-in amplifiers are designed in current-mode. It gives the advantage, that currents can be driven with lower voltages. This enables high-precision measurements at higher frequencies [Grimnes and Martinsen (2000), Min and Parve (1996a, 1997)]. Recently there has been development of mixed signal measurement systems, using analog-mode for measurement and digital-mode for signal processing [Min et al. (2001), Gordon et al. (2005)].

2.5 Implanted measurement devices

Implanted bioimpedance measurement devices are used in cardiac pacemakers and defibrillators [Webster (1995)]. They can also be used for monitoring of the health of other organs after major surgery or transplantation. Implantable measurement devices have severe limitations compared to regular equipment. Most notable of the imposed limitations are size, weight, outer materials and autonomy. The device has to be as unnoticeable to the patient as possible. The measurements should also not be interfered by body signals and should not interfere with the

functions of the body and other equipment. All other limitations are derived from those basic requirements. The parts that come in contact with the host organism (patient) have to biologically compatible and harmless [Webster (1995)]. This includes the case of the device, leads/wires, electrodes and other possible parts and sensors. The device has to include a state-of-the-art battery to be able to work independently inside the patient for up to 10 years [Webster (1995)]. This creates challenges of energy efficiency. Certain parts of the equipment that are not required to work at that moment should be turned off. This feature is desirably implemented also in the impedance measurement part. The circuitry that inserts current, measures voltage and processes the data should be turned on only when necessary. If a cardiac pacemaker detects a necessity to measure impedance, it can turn on the required part and measure at several instances during one cardiac cycle. It may have to be switched off during the pacing pulse phase to protect the sensitive measurement equipment. The energy constrained scenario also gives advantages to different measurement methods, like current mode vs. voltage mode measurement, analog vs. digital measurement and analog vs. digital signal processing [Min et al. (2002), Yufera et al. (2002)].

2.6 Contact problem

Skin has a top layer called ”stratum corneum”. The stratum corneum has a contact with outside world and performs temperature and moisture regulating and breathing functions. Because of these functions, the impedance of the skin is variable [Grimnes and Martinsen (2000), Nicander and Ollmar (2000)]. Because of skin's relative dryness compared to internal structures, it has cooperatively high impedivity. When studying the impedance of internal structures, the existence of the skin typically inhibits the performance of non-invasive impedance measurements. To compensate the skin effect, higher frequencies have to be used and skin impedance at that location and time has to be taken into account. On the other hand, the variability of the skin impedance makes it a great study subject and a good indicator for various body conditions (skin cancer diagnosis [Åberg et al. (2003)], sports activity, sweating).

In case of implanted electrodes, materials used in other engineering applications are not functional. Organism is a very active environment and implanted devices must minimize and accept the reaction of the body. Porous surface-materials

have been used on electrodes to maximize the electrical contact with the tissue. The organism also tries to inflammate and encapsulate foreign objects. This becomes a problem to the electrodes because it decreases their efficiency. Steroid eluting electrode materials have been used to combat that effect and keep the electrodes clean and efficient for electrical contact [Webster (1995), Bolz et al. (1993)].

One way to mitigate contact issues is to use three- or four-electrode measurement technique instead of two. With two electrodes, the same electrodes are used for current insertion and voltage measurement (or vice-versa). With four electrodes, two electrodes are used for generating the field inside the study object and other two are used for measuring the potentials at desired locations. This complicates the measurement setup, but it may allow more accurate measurement because the field at the location of measurement is more uniform and less dependent on the contact between the object and the measurement electrodes. Often four-electrode method is preferable in implanted measurement scenarios because the inflammation and encapsulation has less effect. The three-electrode method shares one electrode for current insertion and measurement [Grimnes and Martinsen (2000)].

2.7 Measured tissue impedances

Historically researchers have received quite different results when measuring impedances of specific tissues. A good compilation of historical material, measured impedances and modelled results are published by C. Gabriel, S. Gabriel, E. Corthout and R.W. Lau [Gabriel et al. (1996a, b, c), Gabriel and Gabriel]. Measured impedance of cardiac muscle has also been published by [Jang-Zern et al. (2002), Steendijk et al. (1993, 1994)].

A notable work was done in 1957 by Schwan [Schwan (1957), Bourne et al. (1996), Grimnes and Martinsen (2000), Ivorra (2003)]. He described the alpha, beta and gamma dispersion regions in the dielectric permittivity graph. A good representative is a muscle tissue that has three clearly identifiable dispersion regions. The following table Table 2.1 shows the main dispersion regions and the physics behind the phenomena [Grimnes and Martinsen (2000), Ivorra (2003),

Table 2.1: Dielectric permittivity regions and mechanisms.

Type	Characteristic frequency	Mechanism
α	mHz - kHz	Counter ion effects (perpendicular or lateral) near the membrane surfaces, active cell membrane effects and gated channels, intracellular structures (e.g. sarcotubular system), ionic diffusion, dielectric losses (at lower frequencies the lower the conductivity)
β	0.1 - 100 MHz	Maxwell-Wagner effects, passive cell membrane capacitance, intracellular organelle membranes, protein molecule response
γ	0.1 - 100 GHz	Dipolar mechanisms in polar media such as water, salts and proteins

Foster and Schawn (1989), Pethig (1984)]. Figure 2.1 shows the dispersions on a dielectric permittivity graph of a muscle tissue and includes the impedance information (in the format of special admittance in this case, as the graphic rises at higher frequencies). Impedance has similar dispersions as dielectric permittivity, but the relationship is more complex. Permittivity is therefore often preferred for dispersion studies [Grimnes and Martinsen (2000)].

All tissues used in the heart modelling in this thesis have an admittivity graph that is rising with frequency increase. This phenomenon introduces a phase-shift in the measured impedance response. Phase-shift would be zero in those frequency ranges where the admittivity graph is level (exhibits no change with frequency increase). The zero-phase-shift case represents a purely resistive response. Let's suppose an impedance measurement scenario, where an AC current of fixed amplitude is input into a sample tissue and a voltage between the electrodes is measured. If the admittivity graph of that tissue at that frequency would have a 45-degree angle rise (on logarithmic frequency and logarithmic admittivity scale), the phase of the measured voltage would trail after the input current by 90-degrees. The 90-degree phase-shift represents a typical behaviour of a capacitor.

2.8 Equivalent circuit models

The basic assumption is that the impedance characteristic of a tissue can be successfully modelled with a simple electrical circuit composed of resistors and capacitors.

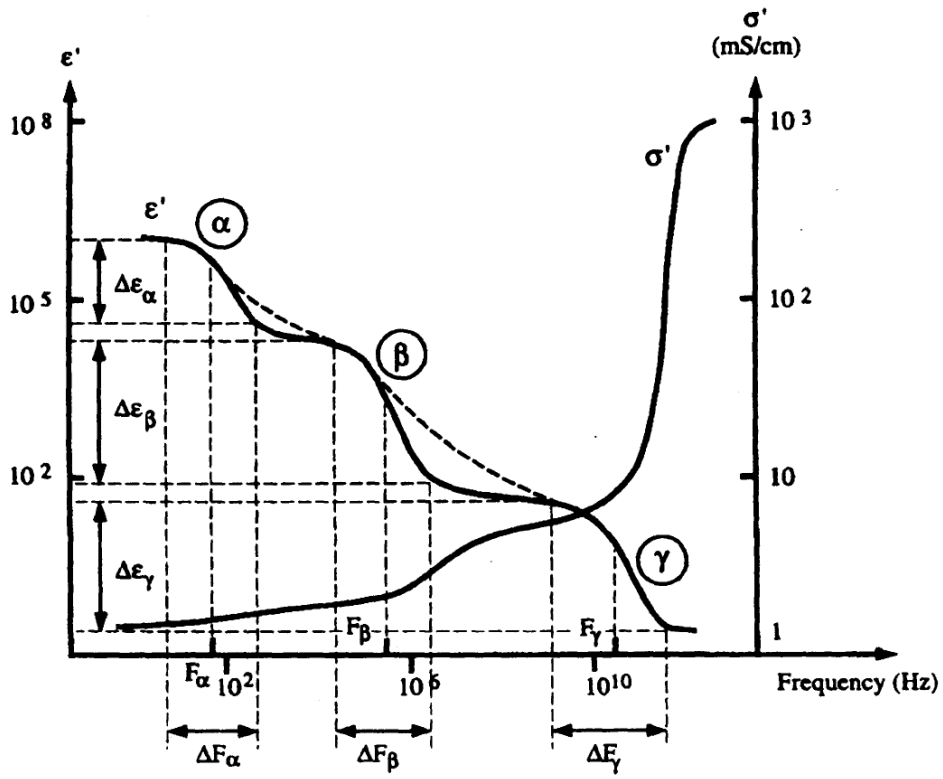

(reproduced from Bourne et al, 1996)

Figure 2.1: Frequency dependence of dielectric permittivity and admittivity of muscle tissue.

Basic idea of the modelling concept of the tissue electrical properties is given on Figure 2.2. Low frequency current can pass only through extra-cellular media, but higher frequencies can also penetrate the cellular walls. Therefore at higher frequencies tissues have lower impedances. Cellular membranes act as capacitors, allowing higher frequency current to pass more easily and also create a phase shift in the current.

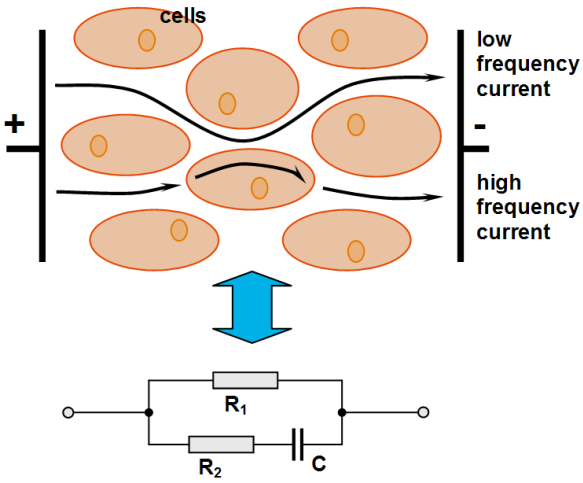

Figure 2.2: Basic principle of a tissue electric equivalent.

Having only one capacitor, this 3-element circuit can model only a limited frequency range that includes just one dispersion. Even in that limited frequency range an actual tissue can not be modelled perfectly with such a simple circuit. This circuit produces an admittance characteristic with a narrow dispersion and the middle section of the dispersion has a 45-degree angle on the log-log scale. In biological tissue the dispersion is usually spread out more widely and a 45-degree response curve of a capacitor is not satisfactory. A simple solution to this was provided by Cole and Cole [Cole and Cole (1941), Zhang et al. (1995)]. They introduced an extra parameter α as addition to the formula of regular electric components. This effectively spread out the dispersion in a wider frequency range. The complex admittance of the circuit is now calculated by the following formula:

$$\dot{Y} = \frac{1}{R_1} + \frac{1}{R_2 + \frac{1}{(i \cdot C \cdot 2 \cdot \pi \cdot f)^{\alpha}}} \tag{2.1}$$

where α is the dispersion value and f is the frequency used for simulation. The

original Cole-Cole model used α-1 in place of only α here. Equation (2.1) was used for modelling tissue impedances in this thesis however. The α parameter therefore has a slightly different meaning here as the one used in the original Cole-Cole model [Cole and Cole (1941)].

2.9 Electro-quasistatic problem, complex numbers

The problem described in this thesis lies somewhere between electrostatics and electrodynamics. With real flowing currents and capacitive effects it is definitely more complex than electrostatics. At the same time we would like to do calculations with simpler methods than the full Maxwell's equations of electrodynamics. In the mathematical model of electrostatics, there is no conduction, convection or impressed currents since electrostatic fields exist only in non-conductive media [van Rienen (2001)]. Quasistatic would be a slightly more complex system where currents are allowed, but capacitive component of tissue impedance can be neglected and electromagnetic propagation effect is also negligible [Malmivuo and Plonsey (1995), Plonsey and Heppner (1967)]. In some cases the time-derivative of magnetic flux is negligible, but the field is predominantly electric and the displacement currents have to be taken into account. In that case it is called electro-quasistatic situation [Motrescu and van Rienen (2005), Clemens et al. (2004)]. We find this situation in bioimpedance measurement scenario.

2.10 Laplace's equation, Poisson's equation

For bioelectric problems without any impressed current source, the electric potential is governed by Laplace's equation:

$$\nabla \cdot (\dot{\bar{\sigma}} \nabla \dot{\phi}) = 0 \tag{2.2}$$

where $\dot{\bar{\sigma}}$ is conductivity of the medium and $\dot{\phi}$ is the electric potential. The line on top of the $\dot{\bar{\sigma}}$ signifies that it can be a rank 2 symmetric tensor. This means anisotropic conductivity of the media. The dots on top of the $\dot{\bar{\sigma}}$ and $\dot{\phi}$ show that the values can be complex [Motrescu and van Rienen (2005), Saleheen and Ng (1997), Saad (2003)].

All the current that is impressed into the system goes to the right-hand side of equation (2.2). This will make a Poisson-type equation:

$$\nabla \cdot (\dot{\bar{\sigma}} \nabla \dot{\phi}) = \nabla \cdot \dot{J}_i \tag{2.3}$$

where $\dot{J}_i$ is complex impressed current density [Motrescu and van Rienen (2005)]. When the region, we are interested, is bounded, boundary conditions need to be set. In case of bioelectric problems, where all current sources and sinks are inside the bounded region, we can set boundary conditions that prohibit any currents through the boundary. This condition is fulfilled by Neumann boundary condition:

$$\frac{\partial \phi}{\partial \vec{n}}(x) = 0 \tag{2.4}$$

where $\vec{n}$ signifies the normal of the boundary surface [Saad (2003)].

2.11 Numerical solution, FDM

When solving this electro-quasistatic problem and the object properties and fields are not given analytically, the solution to the problem is found by a discrete analogue of the Poisson equation [Golub and van Loan (1996), Saad (2003), Wikipedia]. The discrete Poisson equation allows solving the electro-quasistatic problem numerically. The domain or the modelled space is discretized. Each discrete piece in the 3-dimentional model is called an element. It is defined by size and location and in the electro-quasistatic case it also has two electrical properties, admittivity and potential.

Admittivity is a passive property of the material at that location. In electro-quasistatic case it can depend on the frequency of the current passing through and has a complex value. In a general case it is also anisotropic, having different complex values for each direction of the passing current. In a linear approach the admittivity does not depend on the current strength.

Potential can be called an active property, it depends on the specific measurement scenario. When the admittivity and/or the current in the system is complex, then the value of the potential in each element becomes complex also.

Current is another parameter of the system. For discrete elements current can be specified as entering or leaving the system. In those cases those elements are representing electrodes that bring current into the modelling domain. Otherwise the flowing current can not be attributed to elements, it only flows between them.

The discrete Poisson equation is obtained by Finite Difference Method and

gives the following schematic for domain computation:

$$\begin{bmatrix} & & \\ & A & \\ & & \end{bmatrix} \begin{bmatrix} \\ x \\ \\ \end{bmatrix} = \begin{bmatrix} \\ b \\ \\ \end{bmatrix} \tag{2.5}$$

where A is the admittance matrix, x is a column-vector of potentials at each element and b is a column-vector of currents entering and leaving the system through elements. This makes a system of linear equations. x is unknown and we want to find x after solving the system. In a general case the computational domain is a 3D box with $l \cdot m \cdot n$ number of elements. The number of linear equations is therefore also $l \cdot m \cdot n$. Each row of matrix A represents an element and describes how that element is connected to others. Same goes for all the columns. So the matrix A is square and symmetric. Elements of the domain have direct connection only to their neighbours with the maximum number of neighbours for hexagonal elements being 6. This makes the admittance matrix also very sparse and diagonally dominant matrix.

The solution to the system of linear equations is found by an iterative method. Iterative methods allow the solution of much bigger problems than direct solution methods. Conjugate Gradient methods are fast methods for large and sparse matrix equations, but for efficient execution they also require the right preconditioner [Saad (2003)]. A useful preconditioner for large systems is Incomplete Cholesky preconditioner. Finding the right parameters for preconditioning can be done by trial and error. When the optimal speed of the preconditioning plus iterative solution is found, it may often occur that the preconditioning phase is more time- and memory-consuming than iteration.

2.12 Forward problem

In bioimpedance simulation, where the source signal is known (current is inserted by our equipment) and conducting medium is also known but the resulting field is unknown, we are dealing with the forward problem. This source and conducting medium configuration can only produce only one field version. The forward problem has a unique solution [Malmivuo and Plonsey (1995)]. When simulating impedance in a physical object, the accuracy of the result depends on how well do we define the source, how well do we know the conducting medium and how fine

is our discretization.

The first two factors have to do with modelling. We build the model of the source as close as possible to the real source in measurement scenario. Then we build the model of the volume conductor. This includes the geometry, dynamics, conducting properties and properties of the interface with the sources.

The third component in result accuracy, the discretization, gives us choices and is open to more discussion and development. Today it is possible to make discretization very fine to eliminate any errors from this area, but often it is not the most efficient course of action. Sometimes the speed, price or portability of the solver is important enough to justify a controlled margin of error.

2.13 Heart anatomy

The heart is composed of the right heart and the left heart (or just two sides) with two compartments each. In both sides of the heart the atrium is located higher and the ventricle lower (for standing person). The ventricle does the majority of the work and therefore has more muscle mass. From the two sides, the left side of the heart does considerably more work and so the muscle around the left ventricle is the prominent muscle in the heart. Blood enters each side of the heart through the atrium and leaves through the ventricle. Each side of the heart has two valves to regulate the blood flow through the heart chambers. One valve is placed after the atrium (tricuspid valve for the right side and mitral valve for the left side) and the second valve can be found after the ventricle (pulmonary valve for the right side and aortic valve for the left side). Average thickness of left ventricular wall has been measured about 8.0 mm in end-diastolic case and about 12.8 mm in end-systolic case [Troy et al. (1972)]. Muscle thickness at other locations of the heart is considerably smaller. The shape of the ventricles also portrays the load distribution. The left ventricle has a cylindrical shape with circular cross-section. The right ventricle with a thin wall (1-2 mm) is a cup-like formation around the right side of the left ventricle Figure 2.3.

The cardiac muscle cells are extremely short compared to skeletal muscle cells. The length of individual myocardial cell is about 100 μm and thickness about 15 μm. At the ends they are connected to neighbours with gap-junctions, pathways to connect the cytoplasms of the two cells. These gap junctions allow excitation to progress more quickly and provide the timing necessary for proper

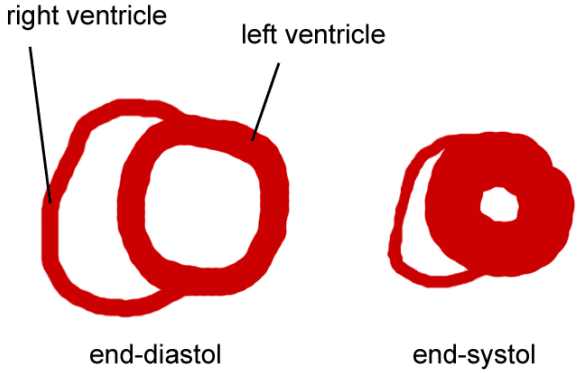

Figure 2.3: Cross-section of the heart during end-diastole and end-systole.

contraction of the myocardium. In addition to the myocardium the ventricles also contain papillary muscles that are located inside the ventricles. The left ventricle contains two and the right ventricle three papillary muscles. The papillary muscles have one end connected to the myocardium and other end holds the corner of the atrioventricular valve. The papillary muscles contract during the shortening of the ventricles to hold the valves in place and not let them flap back into atria [Vander et al. (1990a)]. All four valves in the heart are part of atrioventricular plane that resides almost horizontally in the middle of the heart between the atrias and the ventricles [Slordahl et al. (2004)].

2.14 Myocardial fibre structure

Short cardiac cells chained together form the fibre structure of the whole myocardium. The myocardial fibres are organized in layers around the ventricles. Fibres in each layer do not have the same direction. The epicardial layer and the endocardial layer have a more vertical fibre angle while the middle layer inside the myocardium has a more horizontal fibre angle. The angles are slightly variable in different locations, but the general schematic is shown in Figure 2.4 [Greenbaum et al. (1981), Sengupta et al. (2006), Kocica et al. (2006), Sermesant et al. (2005, 2006)]. In addition to the structure of the myocyte fibres there is also anisotropic structure of collagen fibres present in the myocardium [Coghlana et al. (2006)].

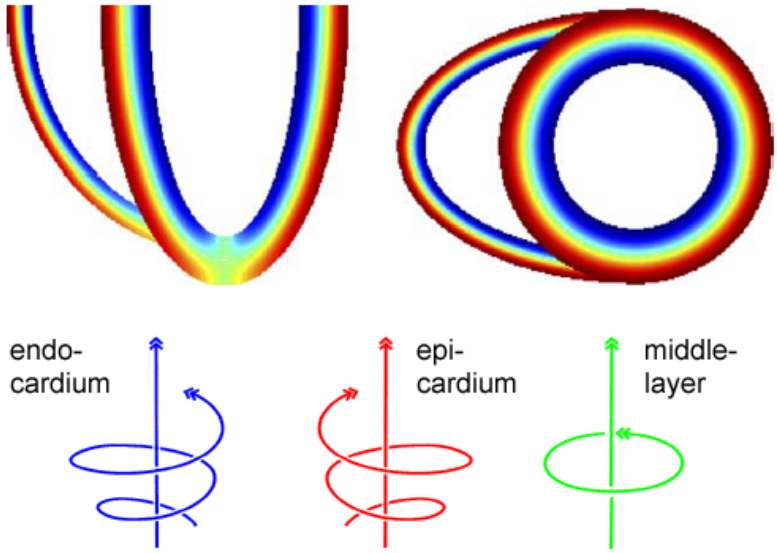

Figure 2.4: Myocardial fibre structure.

2.15 Anatomy dynamics

The heart contracts so that it keeps the stroke volume of the left and the right side equal. If it were not the case, several pathologies would follow. It has been noticed that although the volume of blood that the heart is exerting is considerable, the total heart volume changes very little [Lundbäck (1986), Hoffman and Ritman (1988)]. The volume dynamics of the ventricles has been well recorded and is most conveniently seen in a textbook Figure 2.5 [Vander et al. (1990b)]. The volume dynamics of atrias is less talked about, but they follow a similar curve. The total volume and ejection fraction is comparable to the respective values of the ventricles. The contraction of the atrias happens right before the ventricular systole and increases the filling of the ventricles. The heart is attached to the body from the base where all the blood vessels entering and leaving the heart are located. When atrias contract, they pull the atrioventricular valve plane upward towards the base. This stretches the ventricles vertically and increases their blood content at the end of the diastole. During systole the contraction of the ventricles pull the atrioventricular plane down toward the apex, squeeze the blood into aorta and pulmonary artery and cause rapid filling of the atrias by stretching them

vertically. Diastole begins with fast filling of the ventricles, when ventricles are relaxed and allow the elastic forces in the atrias to pull the atrioventricular plane upward. Other effects that have been noticed in the heart dynamics include a slight twisting of the heart inside the chest (counter-clockwise about 30 degrees) around the axis between the base and the apex. The contraction changes the shape of the heart considerably and therefore the fibre structure of the myocardium must also change. When taking into consideration the propagation of activation (from endocardium towards epicardium as noted [Sermesant et al. (2006), Malmivuo and Plonsey (1995), Durrer et al. (1970)]) the actual contraction of the fibre structure of the myocardium will probably prove to be very complex.

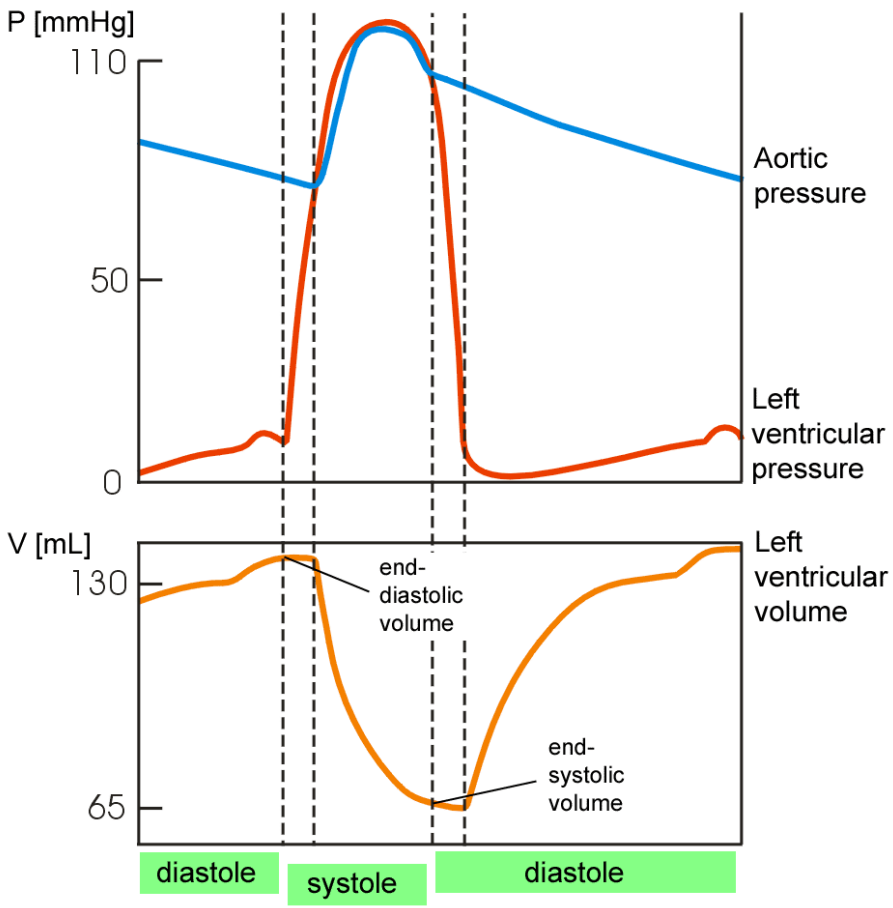

Figure 2.5: Dynamics of left ventricle volume and pressure.

Chapter 3

Materials and methods

3.1 Modelling and simulation pipeline description

This section gives an overview of the whole modelling/simulation process and dataflow. Modelling the heart and tissues and conducting the simulation can be done in the following order:

- Creating static heart geometry model (creation of spline surfaces from slice data, corrections for accurate volume and muscle thickness);
- Animating the geometry by parameters (ejection fraction, volume change characteristic);
- Calculating volumes, then repairing the model;
- Selecting current input electrode locations for each time-frame (one electrode close to left ventricle bottom, other higher in the cavity in respect of that);
- Export spline surface data to volume data, 3D model for each time-frame (create all model data necessary for following steps);
- Tissue properties modelling (blood, muscle and lung impedance), defining measurement frequencies;
- Conductivity matrix generation (generate and store all matrices necessary for next steps, number of matrices equals the number of time-frames times the number of frequencies);

- Solving all the matrices using electrode locations for current insertion (complex-number solver or real formulation);
- Choosing electrode-locations for voltage measurement;
- Visualization of fields, plot of signals, 3D animation of frequency-sweep or dynamics, visualization of Re-Im or Mod-phase signals;
- Using these results in development of flexible whole-organ impedance models (like Cardiac Volume Computer [Salo (2002)]) then back to the 3D modelling/electrode positioning stages.

3.2 Static 3D spline model creation

The initial 3D model was created from crude CT heart data that was generously provided by Department of Physics, the University of Tartu, Tartu, Estonia. This data was manipulated and repaired for cleaner compartment representation. On the slices of this data the surfaces of the epicardium and the endocardium were visible. The images were then manually segmented to have the three tissues (blood, muscle and lung) represented with three colour values. After that additional slices were created manually to fill in the gaps between the initial 6 slices. On the static heart model, composed of slices of 3 colour values, early simulation of intracardiac impedance signals was conducted. The aim was mainly observe the impedance of a whole organ at different frequencies. Electrode placement was only possible to the centres of the voxels of the model volume-data. Experience from those simulation results led to the conclusion, that a flexible heart modelling system is necessary that provides dynamic movement, smooth adjustable surfaces and precise arbitrary electrode placement. Spline surface-functions were then taken into use due to their availability in the MATLAB environment. First on each image (slice of the heart) points on the tissue-boundaries were found with ”contourc” MATLAB function [see Appendix: MATLAB features and capabilities]. The Thin-plate smoothing spline function ”tpaps” [see Appendix: MATLAB features and capabilities] was then used to unite the contour-point data from each slice to a 3D smooth spline surface. The contour finding and 3D spline creation was done for each compartment separately (two ventricles, two atria and epicardium). The spline surfaces were saved as control-point data and smooth-functions in polar coordinates because this provided easier creation of closed sur-

faces. The implementation of polar coordinates required the definition of a centre point for each compartment. The ”tpaps” spline function did not permit multiple radius data for one angle in polar coordinates. Therefore the centre point of each compartment had to be selected carefully to prevent ”folding” of the surface with respect to the centre-point. Finding the right centre point was easy for the more round compartments, like epicardium and left ventricle Figure 3.1. The atrias were a bigger challenge because they also included parts of vessels entering and leaving the heart. Creating the atrias with a smoothing spline function changed the sharper edges of the blood area (atrium and vessels together) considerably. It was not considered a big problem because they reside farther away from the measurement electrodes and consequently contribute little to the simulated signal. For convenience the aorta was modelled as one piece with the left atrium (Figure 3.1) and the pulmonary artery was modelled as one piece with the right atrium (Figure 3.1).

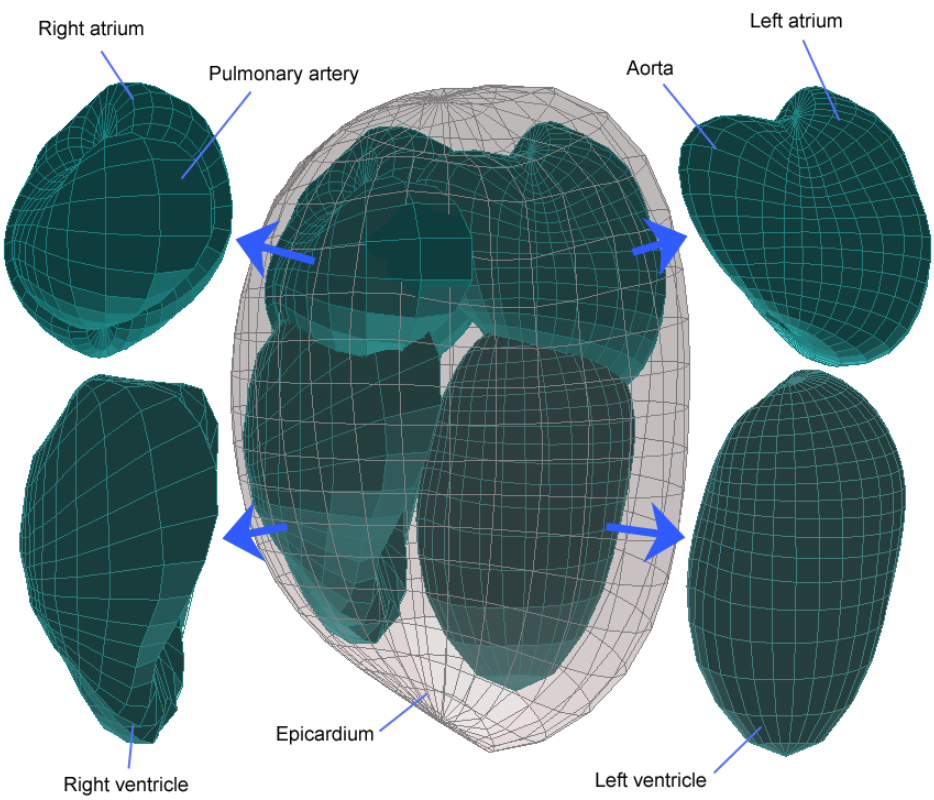

Figure 3.1: Compartments of the spline heart model.

Finding the right centre spot for right ventricle was the hardest. This was due to the cup-like shape of the compartment as it is bent around the left ventricle. The resulting spline retained most of the shape of the original data, but had to cut some of the edges of the right ventricle shorter to avoid them folding behind the middle section (when viewed from the centre point) (Figure 3.1).

3.3 Animating the geometry

A graphic-user-interface (GUI) was created for implementing any necessary modification to the acquired heart shape and animating it. MATLAB feature ”guide” [see chapter Background: MATLAB features and capabilities] was used to create the GUI and all the functions/behaviours of the system were written into the MATLAB code that runs GUI. In effect a cardiac bioimpedance measurement modelling system was created (main dialog on Figure 3.2).

The modelling system exhibits the following features:

- Storing (saving, loading, renaming) of multiple heart models in MATLAB spline format;
- Heart with 4 chambers is composed of 5 closed spline surfaces (4 chambers and epicardium);
- Viewing of the whole heart model and compartments separately from arbitrary angles with zooming;
- Viewing the placement of current insertion electrodes in the left ventricle;
- Editing of the shape of the chambers through separate dialogs ”Edit spline” and ”Smooth area” *;
- Animating a static heart model through separate ”Edit dynamics” dialog *;
- Editing the animation of each chamber through the ”Edit dynamics” dialog *;
- Animated heart is composed of splines closed in space (round objects without gaps) and in time (end of the cardiac cycle is the same as beginning);
- Viewing the animation of the whole heart model and compartments separately from arbitrary angles with zooming;

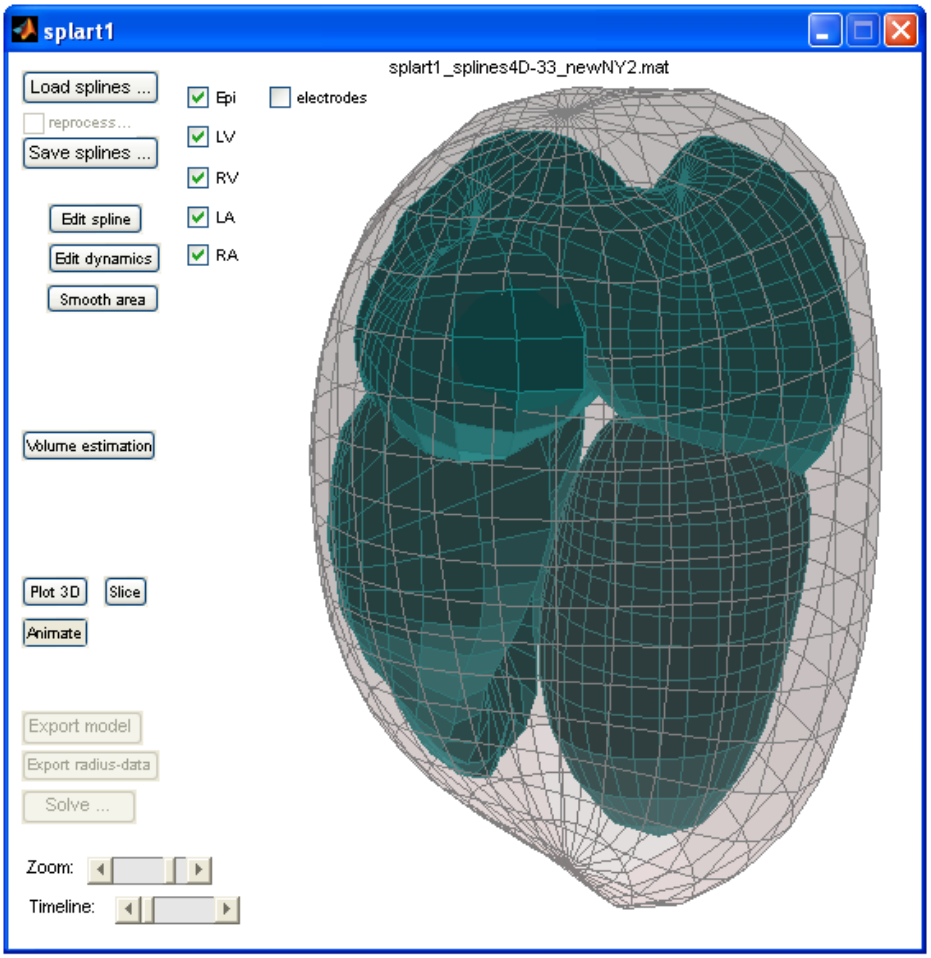

Figure 3.2: The dynamic heart modelling system with a sample heart model file ("splart1_splines4D-33_newNY2.mat") loaded and shown in the main dialog window ("splart1").

- Viewing the motion of current insertion electrodes during cardiac cycle animation;
- Viewing of the heart model at different time-slices of the heart cycle;
- Viewing slices of the heart model like CT images through ”Slice” and ”Volume estimation” dialogues;
- Calculating the volume of the chambers through the whole cardiac cycle through the ”Volume estimation” dialogue;
- Exporting volume data ready for FDM meshing (in bioimpedance simulation calculation) through the ”Volume estimation” dialogue;
- Exporting volume data with different densities (x-y-z resolution and time-frames per cycle);

* *Please note that chambers and epicardium are separate entities. For example, after editing the ventricle surface, epicardium also has to be edited to maintain the thickness of the myocardium at the location.*

We now go through the more important tools in the system, explaining the features and working principles.

Spline-file data format

The heart model data is saved in five MATLAB variables type ”struct” - one for each compartment. The file for one dynamic heart model also includes the centre points for each compartment. The data in ”struct” variables are spline data in spherical coordinates. Radius of the closed round and smooth surface depends on three variables - horizontal angle THETA, vertical angle PHI and time-frame (Figure 3.3). In effect the contraction of a single round compartment model in one heart cycle makes a 4D closed surface. Horizontal angle THETA is composed of 29 control points (30. point repeats the first), vertical angle PHI is composed of 19 control points (20. point repeating the first) and time is composed of 32 control points (33. point repeating the first and closing the cycle). The rest of the angles between the control-points (desired in smooth image creation) are derived from spline-interpolation.

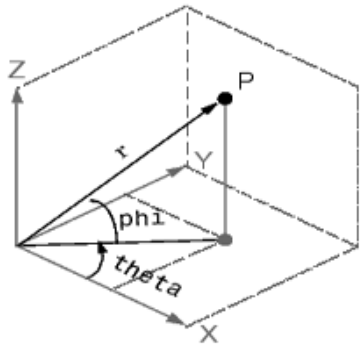

Figure 3.3: Components of spherical coordinates.

Edit spline toolset

Opens from the ”Edit spline” button and allows the editing of the surfaces of each of the five compartments separately. It has a compartment selection menu (epicardium, left ventricle, right ventricle, left atrium and right atrium) and controls-sliders for selecting the size and location of the patch on the compartment we need to edit. A dynamic update of the selected patch area is shown on the spherical drawing in the middle of the toolset. It represents the selected compartment in a simple form. When pushing the ”⇐ Plot” button, the selected patch appears in the main dialog on the selected compartment and has the real shape. The patch area can be lifted out from the surface or pushed in depending on the ”Change magnitude (%)” slider. The ”Smoothing type” selection determines how the raised or lowered patch area is blended with the rest of the compartment. It has three options: normal (as normal distribution, shown active in Figure 3.4), sharp (narrower than normal) and wide (wider than normal). Then graphic next to the menu shows the smoothing profile shape and height as it is raised or lowered from the compartment surface. ”Apply change!” button applies the settings to the compartment and updates the result in the main dialog window. If the compartment had dynamic behaviour, the applied change carried over to all the 32 time-frames. This editing toolset window should be closed from the special ”close” button and not the red cross in the upper right corner of the window.

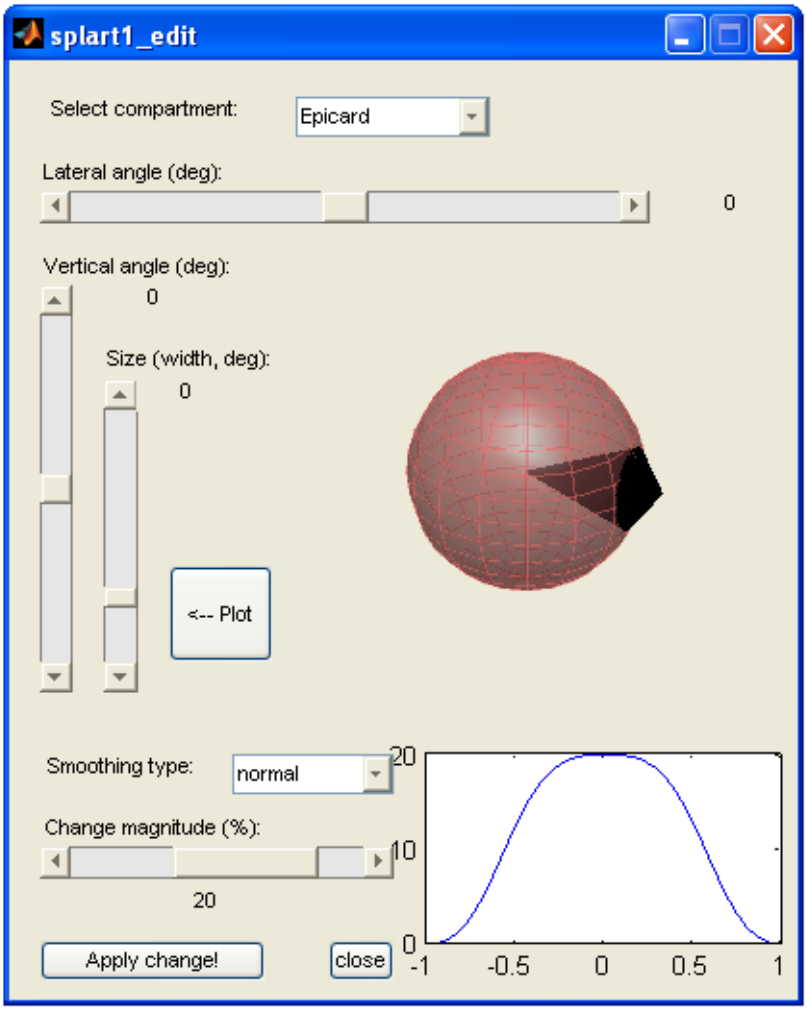

Figure 3.4: The static spline editing toolset. Can also be applied to dynamic compartments.

Edit dynamics toolset

The top row in the ”splart1_editdyn” dialog contains compartment selection menu and feature selection menu (Figure 3.5). Right below those are the sliders for patch selection. A dynamic update of the selected patch area is shown on the drawing in the middle. It represents the selected compartment in a simple form. When pushing the ”⇐ Plot” button, the selected patch appears in the main dialog on the selected compartment and has the real shape. The dynamics can be adjusted with the items in the middle of the window. The ”Shape of dynamics” menu provides different characteristics to add to- or subtract from the motion of the compartment surface during cardiac cycle. It has the following options:

Normal - change function is normal distribution;

Sharp - change function is a faster peak;

Fast fall - change function starts with normal distribution and falls in the faster peak fashion;

Fast rise - change function starts in the faster peak fashion and fall with normal distribution;

Show wobble - implemented for suppressing a wobbling effect, rarely necessary;

Faster fall - change function starts with normal distribution and falls sharply;

Faster rise - change function starts sharply and falls with normal distribution;

Custom - opens a separate dialog where dynamics function can be built with 32 vertical slider in ”graphics equalizer” fashion.

The ”Custom” option has the same effect as pushing the ”Eq.” button. The graphic equalizer window (Figure 3.6) also has the ability of loading an image file for the background. This allows very handy modification of the dynamics with the help of some premade graph. Different custom dynamic forms can be saved and loaded later through this window. The effect of the selected dynamics change option is immediately shown in the figure on the right. The horizontal scale shown 32 time-frames of the cardiac cycle and vertical scale has the magnitude of change. The value is taken from the centre point of the patch selected with the controls above. It shows three lines: bottom line (green) is the change function regardless

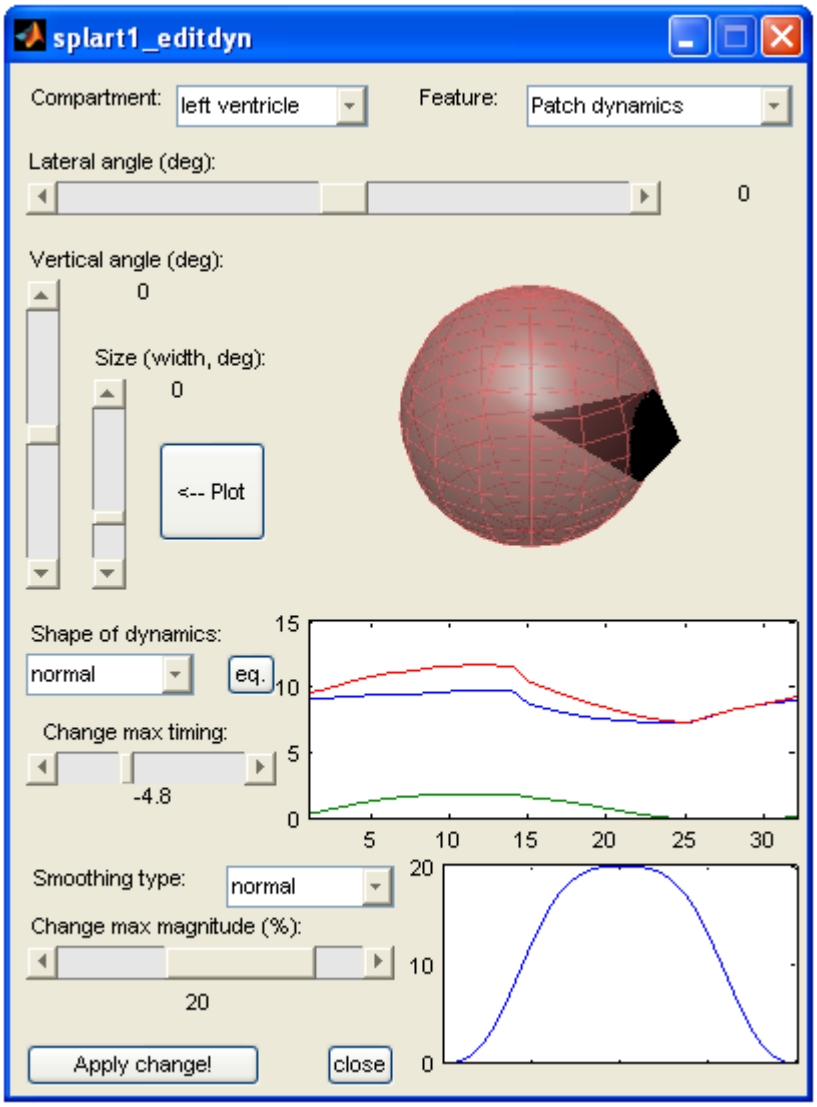

Figure 3.5: The spline dynamics editing toolset.

of the compartment, middle line (blue) shows the original dynamics of the patch centre point and the top line (red) shows the resulting motion of the patch centre point. The timing of the dynamic change form can also be adjusted with the ”Change max timing” slider.

The features menu on the top right provides the following actions that can be performed with all dynamics settings described above:

Patch dynamics - uses the selected patch and dynamics settings to control the motion of a patch;

Remove wobble only - additional smoothing feature if specific wobble is present between odd and even time-frames, rarely needed;

Make patch static - the option of making the selected patch static;

Whole comp. Increase - increasing the compartment with the value taken from ”Change max magnitude (%)” slider, ignores other settings;

Whole comp. Inc. Dyn. - animating the whole compartment and ignoring the patch selection settings;

Whole comp. Static! - makes the whole compartment static for starting the animation process all over, ignores all other settings in the dialog.

The ”Apply change!” button applies the selected feature on the selected compartment with the settings displayed and updates the 3D drawing in the main dialog window Figure 3.2. This dynamics editing toolset window should be closed from the special ”close” button and not the red cross in the upper right corner of the window.

Smoothing tool

The ”Smooth area” tool uses a simple interface to select a compartment, patch location, visualization and a button to apply the smoothing for that patch (Figure 3.7). Smoothing works only for areas that do not have very different radius values on the patch edge.

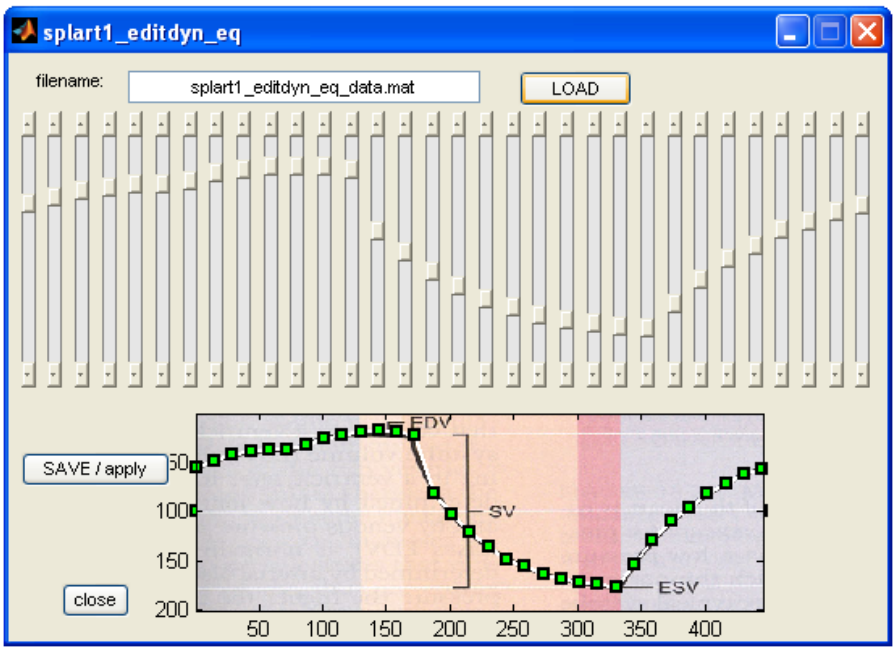

Figure 3.6: The graphic equalizer window with an image from a textbook [Schmidt and Thews (1990)] loaded to the background for help.

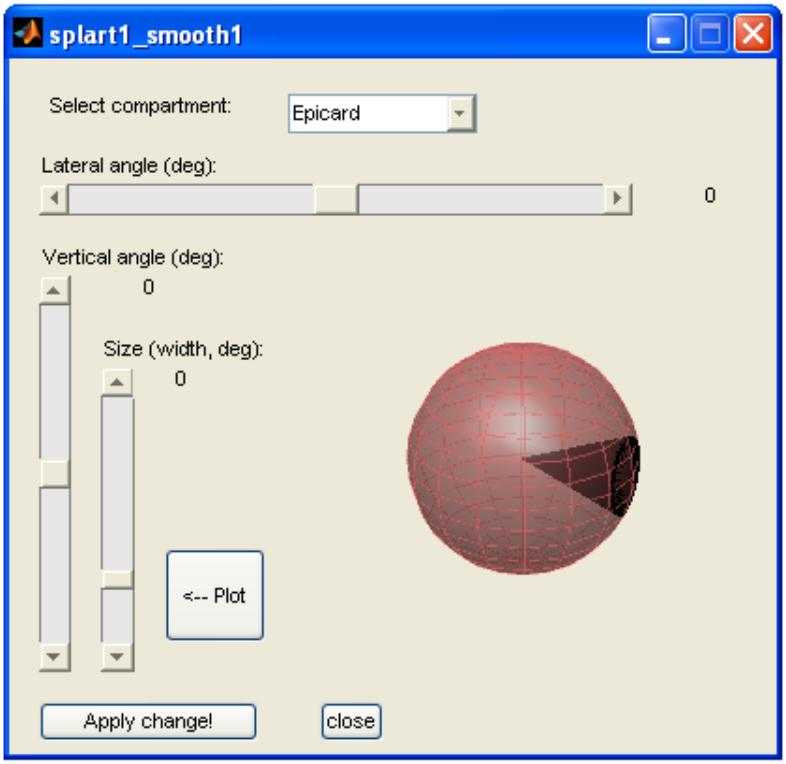

Figure 3.7: Smoothing tool.

Volume estimation toolset

This toolset is used for viewing images of the heart cross-section like Computer Tomography images, computing volumes change characteristics of all compartments and also exporting data for bioimpedance simulation (Figure 3.8). The vertical slider ”Z” controls the horizontal plane through the heart model that we want to visualize. The ”timeline” slider below the drawing selects the exact section of the cardiac cycle that we want to visualize. The ”Compute slice” button shows the selected slice. When the check-box right next to the button is checked, the figure updates automatically whenever the ”Z” slider or the ”timeline” slider is moved. Pushing the ”Animate (slow)” button calculates all the slices on the fixed Z value through the cardiac cycle while showing the progress in the figure. When the check-box next to it is checked, it animates them fast after one slower calculation run like a fast heart-beat. These controls effectively do the same as a small dialog ”Slice” that opens from the main dialog. The only difference is that these here in the volume estimation toolset were developed later and perform much faster.

The controls in the upper right section of the toolset include the essential compartment selection menu and additional fields for resolution parameters. When pushing the button ”Compute compartment volume (ml)”, the toolset starts to go through the slices of that compartment and count the voxels that constitute the volume (also accounting correctly for only partly inside the compartment). The cross-section plot is dynamically updated and shows the progress as the volume of each time-frame is computed. The result of volume calculation is shown in the big graph below. It shows the time-frames on the horizontal axis and volume (in millilitres) on the vertical axis. This graph is updated as the volume of the compartment at sequential time-frames is computed. It can take less than a minute on a 2GHz computer. The Figure 3.8 shows the result of the computation of the left ventricle. The 32 time-frames shown here constitute one cardiac cycle. When calculating the volume of ventricles or atria, the vertical slider ”valve plane” also has a role. It determines a Z value vertically where ventricles end and atria start. By default it is set on a best value for the spline-model included in this presentation. It can be adjusted with the slider and then reset for the default value from the ”reset” button.

Below the graph of volume-dynamics is the ”Export volume data” button. Pushing this button starts the process of making volume data from the spline sur-

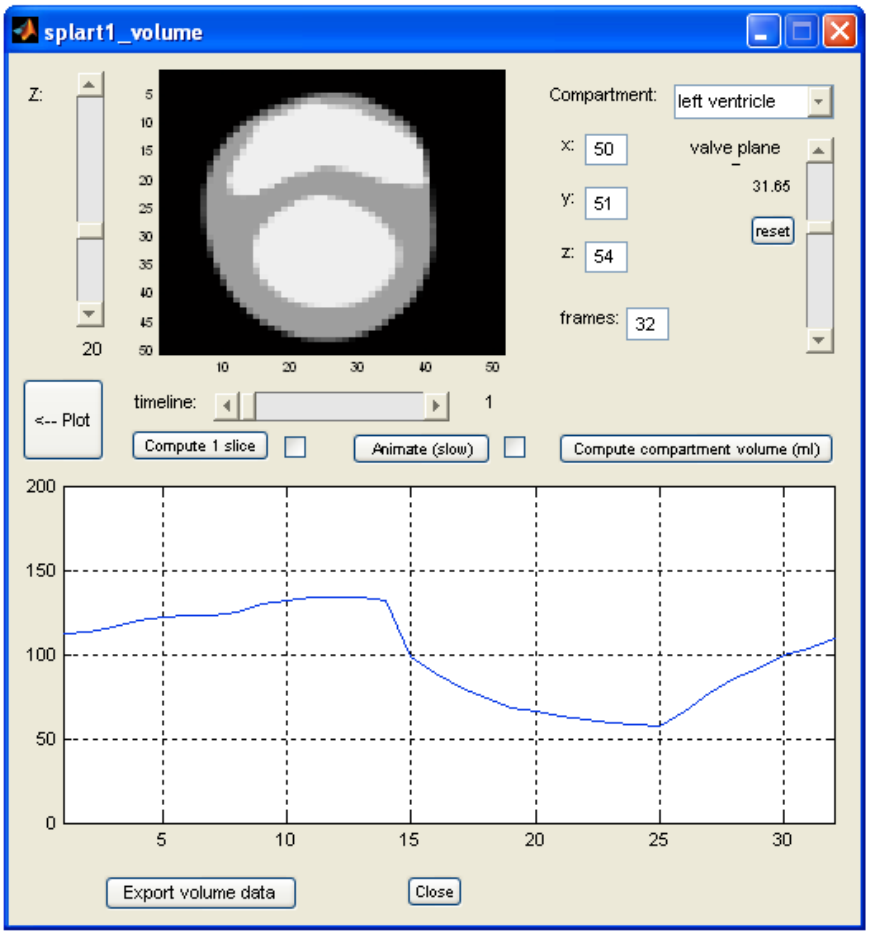

Figure 3.8: Volume estimation and volume data exporting toolset.

faces. While the volume data is calculated, the two graphs on this toolset and the ”Z” slider are updated to indicate the progress of calculation. After the volume data of all the time-frames is gathered, it is saved as ”splart1_VolumeData(50-51-54_32).mat” file. The numbers 50-51-54_32 indicate the 3D resolution of exported data and number of time-frames. These can be changed in the toolset when other resolutions are needed. The exporting can take 10 minutes or more on a 2GHz computer. The datafile ”splart1_VolumeData(50-51-54_32).mat” contains a variable IO with all the volume data for all the time-frames. It is a 4D matrix type variable with dimensions (50, 51, 54, 32). Each value in the file represents a tissue type. The values of tissue types have been defined as 0 for lung, 2 for muscle and 3 for blood. Number 1 has been reserved for fat tissue and fat is not used in this model. During the volume data export many voxels are found to be not fully inside one tissue area. Those voxels are defined as ”between” two tissues and a value is given to them accordingly. For example if half a voxel is in muscle (2) and other half in blood (3), it receives a value 2.5. If $\frac{1}{4}$ of a voxel is in lung area (0) and $\frac{3}{4}$ is inside muscle (2), it receives a value 1.5. The result of volume data export can partly be seen in the top figure as a slice. The edges of the slice are not sharp but blurred in a way that can be called ”antialiasing” in image processing terms. This feature makes the viewing of low-resolution data more pleasant, but it also improves the accuracy (and speed) of FDM computation when this data is used for solving a bioimpedance forward problem.

3.4 Tissue modelling method and actual models used

The frequency dependent admittance of three tissues was used in this thesis: lung, muscle and blood. The source of the admittance data was [Gabriel et al. (1996a, b, c), Gabriel and Gabriel]. Blood and lung tissue data was readily available at their website, but usable heart muscle data (wide frequency scale admittance) was nowhere to be found. Best info on in-vivo heart muscle was found presented by [Steendijk et al. (1993, 1994), Jang-Zern et al. (2002)], but it was not sufficient for creating tissue impedance models usable side-by-side with detailed blood and lung models. Therefore regular skeletal muscle data was used instead of heart muscle.[1]

[1]The author of this thesis is aware that the use of skeletal muscle instead of heart muscle in the experimental runs invalidates the most direct applicability of the impedance simulation results. Still, due to the similarity in the properties of the muscle types, the usability of the modelling system

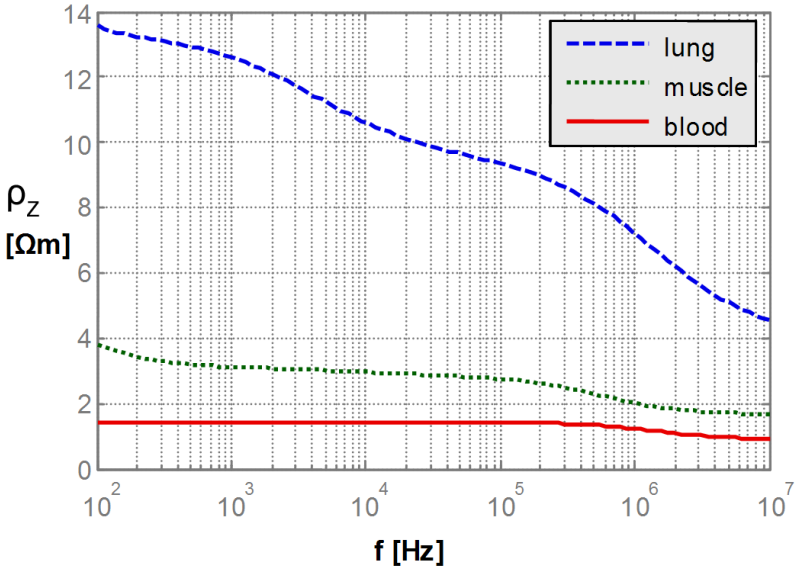

Figure 3.9: Bode plot of the three tissues used in bioimpedance simulation.

The impedance frequency characteristics of the three tissues were used in final simulation as formulas composed of three-element circuit terms (like in chapter Background: Equivalent circuit models, Figure 2.2) and two-element circuit terms (simpler form) with frequency as a variable. The formulas for lung and muscle were composed of 11 electrical elements (resistors, capacitors) and the formula for blood contains 7 elements. In addition to the traditional electrical elements, an α parameter had to be used in the formulations for exact fit as it helps to make the dispersions wider. The Bode plot of the three tissues is shown in Figure 3.9.

Here are the formulas for the special admittances of three tissues with parameters included:

Lung (inflated)

$$Y_{03} = \frac{1}{\frac{1}{\frac{1}{R_{31}}+\frac{1}{XC_{31}}}+\frac{1}{\frac{1}{R_{32}}+\frac{1}{XC_{32}}}+\frac{1}{\frac{1}{R_{33}}+\frac{1}{XC_{33}}}+\frac{1}{\frac{1}{R_{34}}+\frac{1}{XC_{34}}}+\frac{1}{\frac{1}{R35}+\frac{1}{XC_{35}+R_{36}}}}$$

where

can still be demonstrated and conclusions on various aspects of the whole modelling-simulation experience can still be drawn.

$XC_{31} = \frac{1}{1i \cdot C_{31} \cdot w}$	$R_{31} = 21$	$C_{31} = 0.00082$	
$XC_{32} = \frac{1}{(1i \cdot C_{32} \cdot w)^{\alpha_{32}}}$	$R_{32} = 3.8$	$C_{32} = 0.65e-5$	$\alpha_{32} = 0.72$
$XC_{33} = \frac{1}{(1i \cdot C_{33} \cdot w)^{\alpha_{33}}}$	$R_{33} = 5.5$	$C_{33} = 1.5e-8$	$\alpha_{33} = 0.75$
$XC_{34} = \frac{1}{(1i \cdot C_{34} \cdot w)^{\alpha_{34}}}$	$R_{34} = 1.5$	$C_{34} = 1.6e-9$	$\alpha_{34} = 0.78$
$XC_{35} = \frac{1}{1i \cdot C_{35} \cdot w}$	$R_{35} = 2.55$	$C_{35} = 5.4e-11$	
	$R_{36} = 0.043$		

Muscle

$$Y_{33} = \frac{1}{\frac{1}{\frac{1}{R_{61}}+\frac{1}{XC_{61}}} + \frac{1}{\frac{1}{R_{62}}+\frac{1}{XC_{62}}} + \frac{1}{\frac{1}{R_{63}}+\frac{1}{XC_{63}}} + \frac{1}{\frac{1}{R_{64}}+\frac{1}{XC_{64}}} + \frac{1}{\frac{1}{R_{65}}+\frac{1}{XC_{65}+R_{66}}}}$$

where

$XC_{61} = \frac{1}{(1i \cdot C_{61} \cdot w)^{\alpha_{61}}}$	$R_{61} = 1.9$	$C_{61} = 0.00125$	$\alpha_{61} = 0.88$
$XC_{62} = \frac{1}{(1i \cdot C_{62} \cdot w)^{\alpha_{62}}}$	$R_{62} = 0.3$	$C_{62} = 8e-5$	$\alpha_{62} = 0.7$
$XC_{63} = \frac{1}{(1i \cdot C_{63} \cdot w)^{\alpha_{63}}}$	$R_{63} = 1.1$	$C_{63} = 3e-7$	$\alpha_{63} = 0.9$
$XC_{64} = \frac{1}{(1i \cdot C_{64} \cdot w)^{\alpha_{64}}}$	$R_{64} = 0.4$	$C_{64} = 1.55e-8$	$\alpha_{64} = 0.8$
$XC_{65} = \frac{1}{1i \cdot C_{65} \cdot w}$	$R_{65} = 1.3$	$C_{65} = 1e-10$	
	$R_{66} = 0.0136$		

Blood

$$Y_{43} = \frac{1}{\frac{1}{\frac{1}{R_{81}}+\frac{1}{XC_{81}}} + \frac{1}{\frac{1}{R_{82}}+\frac{1}{XC82}} + \frac{1}{\frac{1}{R_{83}}+\frac{1}{XC_{83}+R_{84}}}}$$

where

$XC_{81} = \frac{1}{(1i \cdot C_{81} \cdot w)^{\alpha_{81}}}$	$R_{81} = 0.505$	$C_{81} = 2.7e-7$	$\alpha_{81} = 0.94$
$XC_{82} = \frac{1}{(1i \cdot C_{82} \cdot w)^{\alpha_{82}}}$	$R_{82} = 0.13$	$C_{82} = 3.5e-8$	$\alpha_{82} = 0.9$
$XC_{83} = \frac{1}{(1i \cdot C_{83} \cdot w)^{\alpha_{83}}}$	$R_{83} = 0.78$	$C_{83} = 1.4e-10$	$\alpha_{83} = 0.95$
	$R_{84} = 0.014$		

The parameters for the equations were derived manually to fit the characteristics of the source data exactly. All of those tissue formulas produce accurate results (same as source data) in a frequency range from 10 Hz to 1 GHz.

3.5 FDM matrix generation

The admittivity matrix was created with a custom script in MATLAB program. It reads in the IO variable (4D matrix) from the volume data file ("splart1_VolumeData(50-51-54_32).mat"), takes the first time-frame (3D matrix volume data with resolution 50-51-54) and starts filling the 2D admittance matrix (size 50*51*54 square matrix).

The rows of the matrix are numbered as elements in the discretized domain. The columns are numbered the same way. Each value in the matrix represents admittance between the element with the row index and the element with the column index. Those locations in the matrix, that have no connection between the row-element and the column-element, have zero value. The matrix is a symmetric square matrix with very few non-zero elements.

For accurately filling in the admitting connections between two elements (mesh nodes) it also needs the admittance values of the tissues defined in the volume data at those locations. The admittance of the elements is taken from special admittance formulas of the three tissues. When an element is between pure tissue types (tissue index not exactly 0, 2 or 3 in volume data file), the admittance of that element is calculated accordingly: proportionally between the admittances of the two tissues.

At the location of the matrix (row-element, column-element) a value of average admittance of the two elements is inserted with a negative sign. At the main diagonal of the matrix a positive value is inserted as a sum of all the row elements (same as a sum of all the column elements).

The large and sparse admittance matrix is generated for every frequency of impedance simulation and every time-frame of the cardiac cycle. The structure of the matrix depends on the indexing scheme of the elements. With the simplest indexing it becomes a band matrix with only 7 bands of nonzero elements. Nonzero elements can be found in the main diagonal, in the two diagonals adjacent to it, then in two diagonals at the distance 50 (x-dimension) on both sides from the main diagonal and lastly in two diagonals at the distance 50*51 (x-dimension times y-dimension) from the main diagonal. The 50*51*54 square matrix (137700 elements) contains only 947879 nonzero elements (0.005 %).

3.6 Solving the matrix equation

To solve the matrix equation

$$\begin{bmatrix} & & \\ & A & \\ & & \end{bmatrix} \begin{bmatrix} \\ x \\ \\ \end{bmatrix} = \begin{bmatrix} \\ b \\ \\ \end{bmatrix}$$

to find column vector x, the column vector b has to be defined. This vector contains the currents going in and coming out of the system. Elsewhere b is a zero vector, only in the locations where electrodes were defined (index of electrode elements is given by the spline modelling system in the volume data file) does it have a value. The current value used in all the simulations is 10 μ A. It is a standard current allowed in implanted devices by Medical Safety Standards (*IEC 60601-1 Medical electrical equipment - Part 1: General requirements for basic safety and essential performance*). One of the electrode locations is chosen as a positive electrode location, where current is entering (value 10e-6), the other is chosen as a negative electrode location (or zero), where current is leaving the system (value -10e-6). Before solving the row and column of the element, where the negative electrode was defined, are to be cut out of the A matrix. The appropriate element is also to be cut out from the x vector (unknown) and the b vector. This leaves the system size to be solved at 137699 linear equations.

Solving the system with an efficient cgs method (Conjugate Gradient Squared) requires preconditioning the A matrix. Preconditioning is done by the MATLAB program cholinc (Incomplete Cholesky Preconditioner). The cholinc preconditioner uses a drop-tolerance parameter and in MATLAB platform it gives best results to use the value 1e-3 as a drop-tolerance (for this size system and this particular matrix structure). The cholinc preconditioner generates a preconditioning matrix M that has the same size as A, but consists of many more nonzero elements. The M matrix must be calculated for every new A matrix, it is temporary and should be erased after the solving to save space.

The solving command is cgs. It needs the A matrix, the b vector and the preconditioner M as input. Parameters like tolerance (solution accuracy when to stop) and number of maximum iterations can also be set. A good tolerance is 1e-7. 100 is a reasonable number of maximum iterations for this bioimpedance problem. As an output the cgs gives the x column vector. It can also give additional

info on how the solving went exactly [see Appendix: MATLAB features and capabilities]. This can be useful when debugging or finding optimal parameters for preconditioning and solving.

After solving is done and the cgs method converged, we have a vector with 137699 elements that contains the potentials (in voltages) for all the 50*51*54 elements of the discretized domain except one. The one element left out is the element of the electrode that was defined as negative or zero where the current was leaving the system. By defining the element of the ground electrode we defined it as zero potential and all the other potentials are in reference to that. So we can insert the zero potential value back in and get potential values for all the 50*51*54 elements.

From the vector of potentials (137700 elements) volume data is reconstructed with the help of element indexing info.

For the problem size of 50*51*54 nodes a balance was found between preconditioning and solving to facilitate optimal overall solving time and computer memory consumption. With this selection of parameters (namely cholinc preconditioning drop-tolerance of 1e-3) the preconditioning takes 10 minutes and uses almost a gigabyte of memory while cgs-solving takes 5 minutes and uses only half the amount of memory (calculating times on a 2GHz computer). So overall solving time is around 15 minutes. For example if 10 different frequencies have to be simulated and we want to see the cardiac dynamics over 20 time-frames, we need to create and solve 200 matrices. On a bigger research project where 10 different scenarios of cardiac dynamics (for example ejection fractions) need to be compared over 10 different frequencies with 30 timeframe accuracy, the amount of matrices to solve increases to 10*10*30=3000. That kind of research project would take 750 hours or about a month on a desktop PC if more efficient computation methods are not found.

Chapter 4

Results

4.1 Overview of published and presented work

The studies presented here were not carried out in this particular order, they are numbered for easier following of the thesis. The first study demonstrates the modelling and simulation. The second and third studies explain some aspects of the first study in more detail. The fourth study shows where the modelling system was used. The fifth study validates some of the methods used in the simulation.

4.1.1 Study nr. 1: Simulation of Intra-Cardiac Catheter Complex Impedance Signals with Variable Stroke Volume

The heart modelling system and the impedance simulation method have been used in basic research to demonstrate the intracardiac complex impedance signal behavior with various ejection fractions of the same heart. The description of the virtual experiment and results were presented in a conference of The IEEE Engineering in Medicine and Biology Society in 2006 [see *Appendix I: Simulation of Intra-Cardiac Catheter Complex Impedance Signals with Variable Stroke Volume*].

This study was carried out by me alone. It had several smaller goals. It was conducted to test and demonstrate the capability of the heart modelling system in creating dynamic heart models with very specific characteristics (stroke volume, left and right heart volume balance). This task was completed successfully and it's results are shown on Figure 4. and Table 1. of the article. Although the modelling system enabled to create the 5 necessary models out of one reference

in one afternoon, the modelling procedure (change contraction magnitude, calculate volume curve, change again, recalculate volume...) could be made more automatic. This study was also conducted to test the capability of the modelling system to accurately position electrodes in the left ventricle (LV). The dynamics of the myocardium from time-frame to time-frame were smooth, but the FDM mesh was discrete and electrodes can only be placed to the nodes of the FDM mesh. In some previous simulations the electrodes were made to jump node-to-node to stay at the right distance from LV bottom. That positioning method created ”jumps” in the simulated impedance signal. To guarantee the correct positioning of the electrodes, the position of the LV bottom was fixed in the FDM mesh and the rest of the heart model was made to move in the modelling domain as dictated by the dynamics. This allowed to fix the position of the electrodes with respect to the LV-bottom. The resulting simulated impedance signals were smooth and without jumps that were present in the previous simulations. These findings show the effectiveness of the modelling system to create dynamic heart models that was one of the aims of this thesis.

The impedance signals shown in Figure 5. of the article are not yet ready for comparison with signals from in-vivo measurements because of several reasons discussed in the article (modelling inaccuracies). Furthermore, the signals simulated in this study are taken from the excitation electrodes (2-electrode measurement). This is not a common practice in implanted bioimpedance measurement and it also maximizes the short-comings of FDM ([see *Appendix V: Accuracy of numerical methods in solving static and quasistatic electric fields*]). Practically much more valuable measurement scenario, the 4-electrode method, was not used in this study because the positions for all the 4 electrodes were not known at the time, the heart model was not accurate enough near the base and that simulation would have required the modelling of a much larger area of the chest.

The conclusion from this would be that the modelling of bigger structures (perhaps the whole chest) is going to be necessary. So far in the simulations the positioning of the electrodes was constrained to the LV-cavity. In bioimpedance experiments on live isolated pig hearts (that is planned to be conducted in our laboratory) some of the electrodes are going to be placed on the epicardium and other highly conductive objects could be in contact with the heart. The electrodes of implanted cardiac devices can also be in various places inside and around the heart, even outside the ribcage (the case of the pacemaker). In all of these cases

the modelling of additional structures is going to be necessary.

4.1.2 Study nr. 2: Simulation of Intra-Cardiac Complex Impedance Signals for Developing Simple Bio-impedance Models for Cardio-Dynamics

The results of dynamic heart impedance simulation on a Nyquist plot and how the performance of simple electric equivalent circuits compare to FDM simulation results was presented at the Baltic Electronics Conference 2006 [see *Appendix II: Simulation of Intra-Cardiac Complex Impedance Signals for Developing Simple Bio-impedance Models for Cardio-Dynamics*].

This study was carried out be me alone. The goal of this study was to provide a first comparison between simple models (electric equivalent circuits, Cole-Cole models [Cole and Cole (1941)]) and 3D dynamic heart models. The simulated dynamic impedance signal had not been viewed before side-by-side with dynamic Cole-Cole models. Although the Cole-Cole model is given by a simple equation, the bioimpedance signal gets very complicated once the model is made dynamic. No attempt was made to adjust the simple model to generate the same dynamic signal as the 3D dynamic heart model. That was because to my experience the positioning of electrodes in the heart has great effect on the simulated bioimpedance signal and the possible positions of real electrodes of implanted bioimpedance devices were not known exactly at the time of the study. This study was conducted to further highlight the usefulness of the modelling and simulation system as an aid in finding simple impedance models for practical applications. It is meant as an addition to the initial goals of the thesis and as an step towards future research. This study helped me to come to the following conclusion: simple models of impedance dynamics in the form of Cole-Cole equations can be used for practical applications, although automatic fitting of model parameters will probably be needed.

4.1.3 Study nr. 3: Bio-Impedance FDM-Modelling Inside Heart for Application in Implanted Devices

The effect of anisotropy of the cardiac muscle on the impedance measurement and the issues with anisotropy and FDM are discussed in an article published in Electrocardiology 2004 collection [see *Appendix III: Bio-Impedance FDM-Modelling*

Inside Heart for Application in Implanted Devices]. The results were also presented at the 31st International Congress on Electrocardiology (ICE 2004) in Kyoto, Japan.

The study was carried out by me. Study plan, some writing and presentation at the ICE 2004 congress were done by co-author Alar Kuusik. Initially, during the experimentation with the static heart model, there was a plan to include the structure of myocardial fibres in the heart model. During the FDM discretization of the fibre structure it was evident that FDM simulation was going to have problems with fibres placed diagonally to the mesh. As an addition to the conclusions in the article it should be pointed out once more that in practical cases all the electrodes may not be placed inside the LV cavity. In a general case some electrodes are not immersed in the highly conducting blood and electrode pairs are separated by more tissues. Then the part of the current that penetrates the myocardium is larger and the anisotropy of the fibres possibly plays a bigger role.

This study is another example of a successful virtual experiment that was an aim of the thesis. This virtual experiment assessed possible errors from the anisotropic nature of the myocardium.

4.1.4 Study nr. 4: A Virtual System for Simultaneous Multi-frequency Measurement of Electrical Bioimpedance

The results of using the heart modelling system in a virtual multi-frequency bioimpedance measurement system was published in the International Journal of Bioelectromagnetism in 2005 [see *Appendix IV: A Virtual System for Simultaneous Multi-frequency Measurement of Electrical Bioimpedance*]. Those results were also presented at a conference 5th International Conference on Bioelectromagnetism and 5th International Symposium on Noninvasive Functional Source Imaging within the Human Brain and Heart (BEM & NFSI 2005) in Minneapolis, MN, USA.

The study plan, the LabView software and the electronics were developed by Raul Land, Mart Min, Toomas Parve and Rodney Salo. I provided the visual model of the cross-section of the dynamic heart (Figure 2. in the article), the 3D view of the heart and placement of electrodes (Figure 3. in the article) and the simulated impedance signals that are run in the virtual-experiment-mode of the system (some of them seen in Figure 4. in the article). Conclusions from my role in this study are about the simulation of the signals. As can be seen in Figure 4.

in the article, the simulated signals do not have enough resolution (time-frames) and exhibit ”jumpiness” that was not actually present in the dynamics of the heart model. Similar simultaneous ”jumps” can be noticed in all 3 signals in Figure 4. Those simulations were made before the proper technique for electrode placement was developed. The electrodes were made to jump from node to node in the FDM mesh to maintain a set distance from the LV-bottom during the heartbeat. Experiences during this stage of the modelling hinted that the signal is very sensitive to the distance between the electrode and the endocardial wall. This specific ”jumpiness” of the signal disappeared once I was able to fix the LV-bottom to a node in FDM mesh. This study is another example of a virtual experiment that was an aim of the thesis. This study helped to illuminate a specific weak spot (electrode positioning) in dynamic heart modelling and ultimately bring the modelling quality to the next level.

4.1.5 Study nr. 5: Accuracy of numerical methods in solving static and quasistatic electric fields

The use of Finite Difference Method in bioimpedance was validated and compared to other methods (FEM and analytical method). The results were published in Proceedings of Estonian Academy of Sciences 2006 [see *Appendix V: Accuracy of numerical methods in solving static and quasistatic electric fields*].

The problem and aims of the study were posed by Jari Hyttinen. The study plan was made by me and it was improved in close cooperation with Tuukka Arola. The models for FDM calculation were made by me and the solver that was used for FDM calculations was made by Tuukka Arola. Models and calculations with FEM were done by Katrina Wendel. Models and calculations with the analytical method were done by Outi Ryynanen. This study rouse from a necessity to validate the FDM method and justify it’s use for bioimpedance signal simulation. Any comparison with live experimental data was not possible due to the lack of any such data (together with subject description detailed enough for modelling). Comparison with other methods that have stood against the test of time and are being used in practice gives a good reason to believe in the newly developed method. The results of the study gave real confidence in using the simulation system. During the study a good way was found to implement the size of the electrode. All the elements in the mesh that were supposed to represent an electrode were given a high conductivity value (the conductivity of the actual electrode material) and

the need to insert current to many adjacent mesh nodes disappeared. This study validates the methods of the thesis only partly. Full validation would require an extensive study on how the virtual impedance experiments on virtual hearts compare to real experiments on real hearts. That kind of validation would require the virtual heart be the model of that particular live heart with accurate admittivity parameters and therefore poses serious challenges.

4.2 Discussion

There are fundamentally two ways to use the results of bioimpedance simulation. First would be a direct case, where the positions of excitation electrodes and measurement electrodes are fixed and result signals are needed without in-vivo experiments. This would be a typical solving of the forward problem. It is possibly used for building simpler models for real-time estimation of stroke volume, condition of the myocardium, position of the electrodes or blood hematocrit.

The other way of using the bioimpedance simulation results would be the first steps in basic research of intracardiac bioimpedance. This would include discussion on several topics that have not yet matured scientifically. For example questions like:

- What frequencies would be useful, in what combination?
- What electrode shapes are best for what and where?
- How many parameters to measure, are real numbers or complex numbers enough?
- How to best use the information of phase angle measurement?

Those questions are quite practical in nature and more oriented for development of devices and diagnostic methods. The basic research point-of-view opens more fundamental questions however. The use of complex numbers is definitely an area in bioelectricity research that has not been investigated and comprehended fully in scientific practice. To begin to gain knowledge of the subject matter, we must first deal with the different ways of presenting the simulation results. Most straightforward would be to just look at the signals that are simulated on the electrodes. That is the only information that would be available in real measurement

scenario. In the virtual experiment the information on potentials and currents is available in the whole domain of the simulation. The whole field should be visualized somehow if we want to understand the complex and dynamic situation.

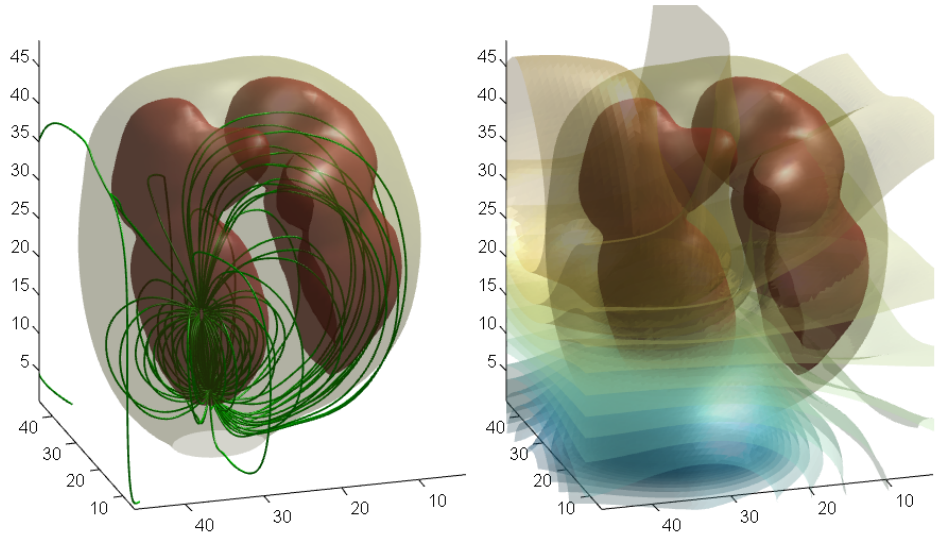

Figure 4.1: Intra-cardiac bioimpedance simulation results shown as current flow-tubes (left) and iso-surfaces of phase angle distribution (right). The heart is viewed from the back, catheter with electrodes is inserted to the left ventricle and the current goes from one electrode to another inside the left ventricle.

Because the 3D heart is dynamic and we are simulating a range of frequencies, we have five dimensions of data to visualize. As we are already accustomed to viewing 3D object on a 2D screen, we could view the other two dimensions with animation. The field of potentials could be shown as moving iso-potential surfaces or current flow-tubes. The animation could be of a single frequency over one cardiac cycle or of a frozen time-frame over the frequency sweep. At the same time we would have to visualize the field of phase angle as iso-potential surfaces. The potential and the phase could be shown side-by-side. Alternatively the potential could be shown as real and imaginary part side-by-side. Ideally all possible combinations of visualizations should be experimented to see what feel more natural and could give productive ideas. One possible way is shown in Figure 4.1, where current flow tubes are shown side-by-side with iso-surfaces of the phase angle. The passage of current through the tissues is pictured by the numerous

flow-tubes. A big bundle of flow-tubes goes through the right side of the heart. It is evident from this image alone that the concentration of flow-tubes could be used to estimate the role of the right heart in the final impedance signal.

4.3 Future studies

The topics of the future studies depend on what projects and scientific collaborations become prevalent in the near future. We have a research partnership project with Basic Research Department of Boston Scientific (USA) on developing the next generation CVC (Cardiac Volume Computer). We have also common interests and ongoing projects with the University of Tartu (Estonia) and Tampere University of Technology (Finland). With these research partners our institute has already conducted successful research on impedance measurement electronics and bioelectric field simulation. Outline of further development includes improving the cardiac modeling system and capabilities of impedance simulation. More specifically, the cardiac modelling system is planned to be made more user-friendly and automatic (automatic control of muscle thickness, dynamics controlled by heart rate). The model of the heart is to be made more realistic in details, especially in the region near the base (atrias, aorta, arteries and veins). The anisotropic structure of the cardiac muscle is to be applied to the modelling system and anisotropic myocardium tissue impedance properties are to be included in future impedance simulations. The heart model (virtual heart) is planned to be modelled as a copy of the heart in a real experiment. This is achieved by implanting ultrasonic crystals (www.sonometrics.com) into the isolated pig heart during live experiments and monitoring the anatomy dynamics during impedance, pressure and flow measurement. The building of new facilities and refitting our institute laboratory is supported by the EU Infrastructure Project.

The more detailed heart models would be complimented with whole thorax models (include breathing, dynamic blood vessels, blood content, pressures and stiffness's of tissues). Bigger developments in this area may need to be conducted in coordination with wide-scale European projects like VIRTUAL PHYSIOLOGICAL HUMAN (Towards Virtual Physiological Human: Multilevel Modelling and Simulation of the Human Anatomy and Physiology, WHITE PAPER, edited by DG INFSO & DG JRC, November 2005
europa.eu.int/information_society/activities/health/docs/events/barcelona2005/ec-

vph-white-paper2005nov.pdf).

The impedance simulation capabilities are also planned to be widened with the introduction of variable mesh density and possibly Finite Element Method computation. More accurate models can also be used in multi-physics modeling (blood-flow in cavities, soft tissues, motion inertia, energy balance). On the other hand, bioimpedance simulation with complex numbers may not satisfy demands in the future and time-domain simulation of electro-magnetics in the chest may become necessary (as a part of multi-physics simulation).

4.4 Conclusions

The aims of the work were achieved:
A computer-modelling system was developed that is capable of designing the heart with different stroke volumes. A dynamic heart model was created containing 4 chambers. The geometry and dynamics are modifiable with the MATLAB-based modelling system. Various virtual experiments (simulations of impedance signal measurement) were conducted on the virtual dynamic heart. The results of the virtual experiments were observed as complex impedance signals originating inside the heart with frequency dependent real and imaginary part. Alternatively they were viewed as signals composed of magnitude and phase information and were visualized as dynamic 3D fields in and around the virtual heart.

Statements:

- FDM computation gives satisfactory results when used in simulation of 4-electrode intracardiac impedance measurement where measurement electrodes reside in blood area. The 4-electrode impedance measurement means here that signals are picked up from electrodes different of those where excitation current is inserted.

- Imaginary part of the impedance signal (or alternatively phase) contains valuable information and helps determine the reason for the behavior of the dynamic signal. Although dedicated state-of-the-art equipment is necessary for measurement of the dynamics of imaginary part (or phase) due to it's small size.

- The adaptiveness and user-friendly modifiability of the heart model is essential for developing simple, medically oriented real-time impedance mod-

els based on virtual experiments.

- The models and modelling systems have to be further improved to rule out errors from unpredicted factors. A fast method of building dynamic 3D models based on physical study object has to be found. This capability would provide means for running real and virtual experiments side-by-side and increase the productivity of research significantly.

Bibliography

Learning MATLAB. The Mathworks, Inc., November 2002. ISBN 0-9672195-7-4.

A. Bolz, R. Fröhlich, and M. Schaldach. Elektrochemische aspekte der electrostimulation - ein beitrag zur senkung des energiedarfs. In M. Hubmann and R. Hardt, editors, *Schrittmachertherapie und hämodynamik*. München: MMV verlag, 1993.

J. R. Bourne, J. P. Morucci, M. E. Valentinuzzi, B. Rigaud, C. J. Felice, N. Chaveau, and P. M. Marsili. Bioelectrical impedance techniques in medicine. *Critical Reviews in Biomedical Engineering*, 24(4-6), 1996.

M. Clemens, M. Wilke, G. Benderskaya, H. De Gersem, W. Koch, and T. Weiland. Transient electro-quasistatic adaptive simulation schemes. *IEEE TRANSACTIONS ON MAGNETICS*, 40(2):1294–1297, March 2004.

H. C. Coghlana, A. R. Coghlanb, G. D. Buckbergc, and J. L. Coxe. The electrical spiral of the heart: its role in the helical continuum. the hypothesis of the anisotropic conducting matrix. *European Journal of Cardio-Thoracic Surgery*, 29:s178–s187, 2006.

K. S. Cole and R. H. Cole. Dispersion and absorption in dielectrics i. alternating current characteristics. *The Journal of Chemical Physics*, 9:341–351, April 1941.

D. Durrer, R. T. van Dam, G. E. Freud, M. J. Janse, F. L. Meijler, and R. C. Arzbaecher. Total excitation of the isolated human heart. *Circulation*, 41:899–912, 1970.

K. R. Foster and H. P. Schawn. Dielectric properties of tissues and biological materials: a critical review. *CRC Critical Reviews in Biomedical Engineering*, 17(1):25–104, 1989.

C. Gabriel and S. Gabriel. Compilation of the dielectric properties of body tissues at rf and microwave frequencies. Internet document. URL: http://www.brooks.af.mil/AFRL/HED/hedr/reports/dielectric/home.html.

C. Gabriel, S. Gabriel, and E. Corthout. The dielectric properties of biological tissues: Ii. literature survey. *Phys. Med. Biol.*, 41:2231–2249, 1996a.

S. Gabriel, R. W. Lau, and C. Gabriel. The dielectric properties of biological tissues: Ii. measurements in the frequency range 10 hz to 20 ghz. *Phys. Med. Biol.*, 41:2251–2269, 1996b. doi: 10.1088/0031-9155/41/11/002.

S. Gabriel, R. W. Lau, and C. Gabriel. The dielectric properties of biological tissues: Ii. parametric models for the dielectric spectrum of tissues. *Phys. Med. Biol.*, 41:2271–2293, 1996c.

G. H. Golub and C. F. van Loan. *Matrix Computations*. The John Hopkins University Press, 1996. ISBN 0801854148.

R. Gordon, R. Land, M. Min, T. Parve, and R. Salo. A virtual system for simultaneous multi-frequency measurement of electrical bioimpedance. *International Journal of Bioelectromagnetism*, 7:243–246, 2005.

R. A. Greenbaum, S. Y. Ho, D. G. Gibson, A. E. Becker, and R. H. Anderson. Left ventricular fibre architecture in man. *British Heart Journal*, 45:248–263, 1981.

S. Grimnes and O. G. Martinsen. *Bioimpedance and Bioelectricity Basics*. Academic Press, London, UK, 2000. ISBN 0-12-303260-1.

R. Hayakawa, H. Kanda, M. Sakamoto, and Y. Wada. New apparatus for measuring the complex dielectric constant af a highly conductive material. *Jpn J Appl Phys*, 14:2039–2052, 1975.

E. A. Hoffman and E. L. Ritman. Intra-cardiac cycle constancy of total heart volume. *Dynamic Cardiovascular Imaging*, 1:199–205, 1988.

B. D. Hoit, N. Ball, and R. A. Walsh. Invasive hemodynamics and force-frequency relationships in open- versus closed-chest mice. *Am J Physiol Heart Circ Physiol*, 273(5):H2528–H2533, November 1997.

A. Ivorra. Bioimpedance monitoring for physicians: an overview. Review, Centre Nacional de Microelectronica, Biomedical Applications Group, 2003. URL: http://www.cnm.es/ mtrans/PDFs/Bioimpedance_for_physicians_rev1.pdf.

T. Jang-Zern, J. A. Will, S. Hubbard-Van Stelle, C. Hong, S. Tungjitkusolmun, B. C. Young, D. Haemmerich, V. R. Vorperian, and J. G. Webster. In-vivo measurement of swine myocardial resistivity. *IEEE Transactions on Biomedical Engineering*, 49(5):472–483, May 2002.

M. J. Kocica, A. F. Corno, F. Carreras-Costa, M. Ballester-Rodes, M. C. Moghbel, C. N. C. Cueva, V. Lackovic, V. I. Kanjuh, and F. Torrent-Guasp. The helical

ventricular myocardial band: global, three-dimensional, functional architecture of the ventricular myocardium. *Eur. J. Cardiothorac. Surg.*, 29:s21–s40, 2006.

S. Lundbäck. *Cardiac Pumping and the Function of Ventricular Septum*. Phd dissertation, Karolinska Institutet, 1986. URL: http://www.grippingheart.com.

J. Malmivuo and R. Plonsey. *Bioelectromagnetism: Principles and Applications of Bioelectric and Biomagnetic Fields*. Oxford University Press, New York, USA, 1995. URL: http://butler.cc.tut.fi/ malmivuo/bem/bembook/index.htm.

M. L. Meade. *Lock-in Amplifiers: Principles & Applications*. Peregrinus, London, UK, 1989.

M. Min and T. Parve. A current mode signal processing in lock-in instruments for bio-impedance measurement. *Med Biol Eng Comput*, 34(suppl 1, part 2): 167–178, 1996a.

M. Min and T. Parve. A current signal processing as a challange for improvement of lock-in measurement instruments. In *XIV IMEKO World Congress*, volume VII, pages 186–191, 1997.

M. Min and T. Parve. Improvement of the vector analyser based on two-phase switching mode synchronous detection. *Measurement*, 19(2):103–111, 1996b.

M. Min, N. Holmström, K. Järverud, R. Land, O. Märtens, and T. Parve. An asic for multifrequency bio-impedance analysis. In *11th Int. Conf. on Electrical Bio-Impedance ICEBI'2001, Oslo, Norway*, pages 251–254, 2001.

M. Min, T. Parve, V. Kukk, and A. Kuhlberg. An implantable analyzer of bio-impedance dynamics: Mixed signal approach. *IEEE Transactions on Instrumentation & Measurement*, 51(4):674–678, August 2002.

V. C. Motrescu and U. van Rienen. Computation of currents induced by elf electric fields in anisotropic human tissues using the finite integration technique (fit). *Advances in Radio Science*, 3:227–231, 2005.

I. Nicander and S. Ollmar. Electrical impedance measurements at different skin sites related to seasonal variations. *Skin Research and Technology*, 6(2):81, May 2000. doi: 10.1034/j.1600-0846.2000.006002081.x.

B. Onaral and H. P. Schwan. Linear and nonlinear properties of platinum electrode polarization. part i: Frequency dependence at very low frequencies. *Med Biol Eng Comput*, (20):299–306, 1982.

R. Pethig. Dielectric properties of biological materials: Biophysical and medical applications. *IEEE Transactios on Electrical Insulation*, EI-19(5):453–474, 1984.

R. Plonsey and D. B. Heppner. Considerations of quasistationarity in electrophysiological systems. *Bull. Math. Biophys.*, 29(4):657–64, December 1967.

P. Åberg, I. Nicander, U. Holmgren, P. Geladi, and S. Ollmar. Assessment of skin lesions and skin cancer using simple electrical impedance indices. *Skin Research and Technology*, 9(3):257–261, August 2003.

Y. Saad. *Iterative Methods for Sparce Linear Systems*. Society for Industrial and Applied Mathematics; 2 edition, April 2003. ISBN 0898715342.

H. I. Saleheen and K. T. Ng. New finite difference formulations for general inhomogeneous anisotropic bioelectric problems. *IEEE Transactions on Biomedical Engineering*, 44(9):800–809, September 1997.

R. Salo. *An Improved Computational Model for Intracardiac Impedance Plethysmography*. PhD dissertation, Kennedy Western University, School of Engineering, 2002.

R. F. Schmidt and G. Thews. *Physiologie des Menschen*. Springer Verlag, Berlin, 1990.

H. P. Schwan. Electrical properties of tissue and cell suspensions. *Adv Biol Med Phys*, (5):147–209, 1957.

H. P. Schwan. Determination of biological impedances. In W.L. Nastuk, editor, *Physical techniques in biological research*, volume 6, pages 323–406. Academic Press, New York, 1963.

H. P. Schwan and C. D. Ferris. Four-electrode null techniques for impedance measurement with high resolution. *Rev Sci Instrum*, 39(4):481–485, 1968.

P. P. Sengupta, J. Korinek, M. Belohlavek, J. Narula, M. A. Vannan, A. Jahangir, and B. K. Khandheria. Left ventricular structure and function: Basic science for cardiac imaging. *J. Am. Coll. Cardiol.*, 48(10):1988–2001, 2006.

M. Sermesant, K. Rhode, G. I. Sanchez-Ortiz, O. Camara, R. Andriantsimiavona, S. Hegde, D. Rueckert, P. Lambiase, C. Bucknall, E. Rosenthal, H. Delingette, D. L. G. Hill, N. Ayache, and R. Razavi. Simulation of cardiac pathologies using an electromechanical biventricular model and xmr interventional imaging. *Medical Image Analysis*, 9:467–480, 2005.

M. Sermesant, H. Delingette, and N. Ayache. An electromechanical model of the heart for image analysis and simulation. *IEEE Transactions on Medical Imaging*, 25(5), 2006.

S. A. Slordahl, O. E. Madslien Valborg, Stoylen Asbjorn, Kjos Arnulf, Helgerud Jan, and Wisloff Ulrik. Atrioventricular plane displacement in untrained and

trained females. *Medicine & Science in Sports & Exercise*, 36(11):1871–1875, 2004.

P. Steendijk, E. T. Van Der Velde G. Mur, and J. Baan. The 4-electrode resistivity technique in anisotropic media: theoretical analysis and application on myocardial tissue in vivo. *IEEE Transactions on Biomedical Engineering*, 40 (11), November 1993.

P. Steendijk, E. T. Velde, and J. Baan. Dependence of anisotropic myocardial electrical resistivity on cardiac phase and excitation frequency. *Journal Basic Research in Cardiology*, 89(5):411–426, September 1994. doi: 10.1007/BF00788279.

B. L. Troy, J. Pombo, and C. E. Rackley. Measurement of left ventricular wall thickness and mass by echocardiography. *Circulation*, 45:602–611, 1972. ISSN print: 0009-7322, online: 1524-4539.

U. van Rienen. *Numerical Methods in Computational Electrodynamics: Linear Systems in Practical Applications*. Springer, Berlin, Germany, 2001. ISBN 3540676295.

A. J. Vander, J. H. Sherman, and D. S. Luciano. *Human Physiology*. McGraw-Hill Publishing Company, New York, 1990a. ISBN 0-07-066969-4.

A. J. Vander, J. H. Sherman, and D. S. Luciano. *Human Physiology*. McGraw-Hill Publishing Company, New York, 1990b. ISBN 0-07-066969-4.

A. I. Vistnes, I. Wormald, S. Isachsen, and D. Schmalbein. An efficient digital phase-sensitive detector for use in electron-spin resonance spectroscopy. *Rev Sci Instrum*, 55:527–532, 1984.

J. G. Webster. *Design of Cardiac Pacemakers*. IEEE Press, New York, USA, 1995. ISBN 0-7803-1134-5.

Wikipedia. Discrete poisson equation. Internet document. URL: http://en.wikipedia.org/wiki/Discrete_Poisson's_equation.

A. Yufera, G. leger, E. O. Rodriguez-Villegas, J. M. Munos, A. Rueda, A. Ivorra, R. Gomez, N. Noguera, and J. Aguilo. An integrated circuit for tissue impedance measurement. In *the IEEE EMBS Special Topic Conference on Microtechnologies in Medicine and Biology*, pages 88–93, 2002.

M. I. N. Zhang, T. Repo, J. H. M. Willison, and S. Sutinen. Electrical impedance analysis in plant tissues: on the biological meaning of cole-cole (alpha) in scots pine needles. *European Biophysics Journal*, 24(2):99–106, October 1995. ISSN 0175-7571. doi: 10.1007/BF00211405.

Chapter 5

Appendixes

Appendix I: Curriculum Vitae

1. Personal data

Name (first name, last name)	Rauno Gordon
Date and place of birth	03.04.1977, Tallinn
Nationality	Estonia

2. Contact information

Address	Kuldnoka 11-95, 10619 Tallinn, Estonia
Phone	+372 5046471
E-mail address	rauno@elin.ttu.ee

3. Education

Institution	Year obtained	Degree
Tallinna Tehnikagümnaasium	1995	highschool
Tallinn University of Technology	2000	bachelor degree in natural sciences
Tallinn University of Technology	2002	masters degree in technical sciences

4. Languages (basic, medium, high level)

Language	Level
estonian	high
english	high
finnish	medium
russian	basic

5. Career

Time of work	Name of organization	Position
1995-1997	AS EOMAP	cartographer
1997	AS Pennu	web-server admin
1998-2000	AS Eesti Telefon	web-server admin
1995-2000	Tallinn University of Technology	student
2000-2002	Tallinn University of Technology	masters student
2002-2006	Tallinn University of Technology	PhD student
2005-2006	Tallinn University of Technology, Doctoral School of Information Technology	researcher
2006-	Tallinn University of Technology, Institute of Electronics	researcher

6. Thesis defended

La2CuO4 struktuursete konstantide arvutamine	2000
Bioimpedants-meetod südametöö analüüsi vahendina	2002

7. Research subjects

bioimpedance, heart and chest modelling, electric field simulation, implantable devices, medical devices

Elulookirjeldus

1. Isikuandmed

Ees- ja perekonnanimi	Rauno Gordon
Sünniaeg ja -koht	03.04.1977, Tallinn
Kodakondsus	Eesti

2. Kontaktandmed

Aadress	Kuldnoka 11-95, 10619 Tallinn, Eesti
Telefon	+372 5046471
E-posti aadress	rauno@elin.ttu.ee

3. Hariduskäik

Õppeasutus	Lõpetamise aeg	Haridus
Tallinna Tehnikagümnaasium	1995	keskharidus
Tallinna Tehnikaülikool	2000	loodusteaduste bakalaureuse kraad
Tallinna Tehnikaülikool	2002	tehnikateaduste magistri kraad

4. Keelteoskus (alg-, kesk-, kõrgtase)

Keel	Tase
eesti	kõrgtase
inglise	kõrgtase
soome	kesktase
vene	algtase

5. Teenistuskäik

Töötamise aeg	Ülikooli, teadusasutuse või muu organisatsiooni nimetus	Ametikoht
1995-1997	AS EOMAP	nooremkartograaf
1997	AS Pennu	web-serveri toimetaja
1998-2000	AS Eesti Telefon	web-serveri toimetaja
1995-2000	Tallinna Tehnikaülikool	üliõpilane
2000-2002	Tallinna Tehnikaülikool	magistrant
2002-2006	Tallinna Tehnikaülikool	doktorant
2005-2006	Tallinna Tehnikaülikool, Info- ja kommunikatsioonitehnoloogia doktorikool	teadur
2006-	Tallinna Tehnikaülikool, Elektroonikainstituut	teadur

6. Kaitstud lõputööd

La2CuO4 struktuursete konstantide arvutamine	2000
Bioimpedants-meetod südametöö analüüsi vahendina	2002

7. Teadustöö põhisuunad

bioimpedants, südame ja rindkere modelleerimine, elektriväljade simulatsioon, implanteeritavad seadmed, meditsiinielektroonika

Appendix II: MATLAB features and capabilities

Here are listed and described some of the standard functions in MATLAB that play the biggest roles in the cardiac modelling and impedance simulation presented here. For keeping the focus, not all of the capabilities of the functions are listed here, just the ones important for the topic. Details on all of the functions can be found in printed MATLAB manuals (for most common functions only, for example in [mat (2002)]), electronic help files supplied with MATLAB software distributions, the MATLAB support centre in the internet
http://www.mathworks.com/support/
and the user community in the internet
http://www.mathworks.com/matlabcentral/.
MATLAB 6.5 (release 13) was used for modelling and simulation in this thesis with additional toolboxes: Image Processing Toolbox, Signal Processing Toolbox and Spline toolbox.

contourc

- low-level contour plot computation. C = contourc(Z,v) computes contours of matrix Z (can be greyscale values of an image file) with contour lines at the values specified in vector v. The length of v determines the number of contour levels. To compute a single contour of level i, use contourc(Z,[i i]). C is a two-row matrix specifying all the contour lines. Each contour line defined in matrix C begins with a column that contains the value of the contour (specified by v and used by clabel), and the number of (x,y) vertices in the contour line. The remaining columns contain the data for the (x,y) pairs.

C = [value1 xdata(1) xdata(2)... value2 xdata(1) xdata(2)...;
dim1 ydata(1) ydata(2)... dim2 ydata(1) ydata(2)...]

Specifying irregularly spaced x and y vectors is not the same as contouring irregularly spaced data. If x or y is irregularly spaced, contourc calculates contours using a regularly spaced contour grid, then transforms the data to x or y.

guide

- displays the GUI Layout Editor open to a new untitled FIG-file. Guide is a very handy utility for creating Graphic User Interfaces for MATLAB code. It produces a ".fig" file, that has all the layout descriptions, and a ".m" file that has contains all the functionality behind the GUI. Although guide automatically creates the files, the ".m" file can later be edited for adding all necessary functionality in MATLAB code.

tpaps

- thin-plate smoothing spline. tpaps(x,y) creates a stform (MATLAB data type) of a thin-plate smoothing spline for the given data sites x(:,j) and the given data values y(:,j). The x(:,j) must be distinct points in the plane, the values can be scalars, vectors, matrices, even ND-arrays, and there must be exactly as many values as there are sites. The thin-plate smoothing spline f is the unique minimizer of the weighted sum

$$pE(f) + (1-p)R(f)$$

with E(f) the error measure

$$E(f) = \sum_j |y(:,j) - f(x(:,j))|^2$$

and $R(f)$ the roughness measure

$$R(f) = \int (|D_1 D_1 f|^2 + 2|D_1 D_2 f|^2 + |D_2 D_2 f|^2)$$

Here, the integral is taken over all of R^2, $|z|^2$ denotes the sum of squares of all the entries of z, and $D_i f$ denotes the partial derivative of f with respect to its i-th argument, hence the integrand involves second partial derivatives of f. The smoothing parameter p is chosen in an *ad hoc* fashion.

tpaps(x,y,p) also inputs the *smoothing parameter*, p, a number between 0 and 1. As the smoothing parameter varies from 0 to 1, the smoothing spline varies, from the least-squares approximation to the data by a linear polynomial when p is 0, to the thin-plate spline interpolant to the data when p is 1.

[f,p] = tpaps(...) also returns the smoothing parameter actually used.

sparse

- generates matrices in the MATLAB sparse storage organization. S = sparse(A) converts a full matrix to sparse form by squeezing out any zero elements. If S is already sparse, sparse(S) returns S. S = sparse(i,j,s,m,n,nzmax) uses vectors i, j, and s to generate an m-by-n sparse matrix such that S(i(k),j(k)) = s(k), with space allocated for nzmax nonzeros. Vectors i, j, and s are all the same length. Any elements of s that are zero are ignored, along with the corresponding values of i and j. Any elements of s that have duplicate values of i and j are added together. Storing matrices in sparse format makes calculation of large systems (like in this thesis) actually possible. All of the MATLAB built-in arithmetic, logical, and indexing operations can be applied to sparse matrices, or to mixtures of sparse and full matrices. Operations on sparse matrices return sparse matrices and operations on full matrices return full matrices. In most cases, operations on mixtures of

sparse and full matrices return full matrices. The exceptions include situations where the result of a mixed operation is structurally sparse, for example, A.*S is at least as sparse as S.

cgs

- Conjugate Gradients Squared method for solving systems of linear equations. x = cgs(A,b) attempts to solve the system of linear equations A*x = b for x. The n-by-n coefficient matrix A must be square and should be large and sparse. The column vector b must have length n. A can be a function afun such that afun(x) returns A*x. If cgs converges, a message to that effect is displayed. If cgs fails to converge after the maximum number of iterations or halts for any reason, a warning message is printed displaying the relative residual norm(b-A*x)/norm(b) and the iteration number at which the method stopped or failed.

cgs(A,b,tol) specifies the tolerance of the method, tol. If tol is [], then cgs uses the default, 1e-6.

cgs(A,b,tol,maxit) specifies the maximum number of iterations, maxit. If maxit is [] then cgs uses the default, min(n,20).

cgs(A,b,tol,maxit,M) and cgs(A,b,tol,maxit,M1,M2) use the preconditioner M or M = M1*M2 and effectively solve the system inv(M)*A*x = inv(M)*b for x. If M is [] then cgs applies no preconditioner.

[x,flag] = cgs(A,b,...) returns a solution x and a flag that describes the convergence of cgs.

Flags can be found in Table 5.1.

Table 5.1: Flags returned by Conjugate Gradient Method.

Flag	Convergence
0	cgs converged to the desired tolerance tol within maxit iterations.
1	cgs iterated maxit times but did not converge.
2	Preconditioner M was ill-conditioned.
3	cgs stagnated. (Two consecutive iterates were the same.)
4	One of the scalar quantities calculated during cgs became too small or too large to continue computing.

Whenever flag is not 0, the solution x returned is that with minimal norm residual computed over all the iterations. No messages are displayed if the flag output is specified.

[x,flag,relres,iter,resvec] = cgs(A,b,...) also returns the relative residual norm(b-A*x)/norm(b), iteration number at which x was computed and a vector of the residual norms at each iteration, including norm(b-A*x0).

cholinc

- Sparse incomplete Cholesky and Cholesky-Infinity factorizations. cholinc produces two different kinds of incomplete Cholesky factorizations: the drop tolerance and the 0 level of fill-in factorizations. These factors may be useful as preconditioners for a symmetric positive definite system of linear equations being solved by an iterative method such as cgs (Conjugate Gradients Squared). cholinc works only for sparse matrices.

R = cholinc(X,droptol) performs the incomplete Cholesky factorization of X, with drop tolerance droptol. droptol is a non-negative scalar used as the drop tolerance for the incomplete Cholesky factorization. This factorization is computed by performing the incomplete LU factorization with the pivot threshold option set to 0 (which forces diagonal pivoting) and then scaling the rows of the incomplete upper triangular factor, U, by the square root of the diagonal entries in that column. Since the nonzero entries U(i,j) are bounded below by droptol*norm(X(:,j)), the nonzero entries R(i,j) are bounded below by the local drop tolerance droptol*norm(X(:,j))/R(i,i). Setting droptol = 0 produces the complete Cholesky factorization, which is the default.

R = cholinc(X,'0') produces the incomplete Cholesky factor of a real sparse matrix that is symmetric and positive definite using no fill-in. The upper triangular R has the same sparsity pattern as triu(X), although R may be zero in some positions where X is nonzero due to cancellation. The lower triangle of X is assumed to be the transpose of the upper. Note that the positive definiteness of X does not guarantee the existence of a factor with the required sparsity. An error message results if the factorization is not possible. If the factorization is successful, R'*R agrees with X over its sparsity pattern.

Appendix III

Simulation of Intra-Cardiac Catheter Complex Impedance Signals with Variable Stroke Volume

Rauno Gordon

Proceedings of the 28th IEEE
EMBS Annual International Conference
New York City, USA, Aug 30-Sept 3, 2006

4 pages

Appendix IV

Simulation of Intra-Cardiac Complex Impedance Signals for Developing Simple Bio-impedance Models for Cardio-Dynamics

Rauno Gordon

Proceedings of Baltic Electronics Conference
BEC 2006
Tallinn, October 2-4, 2006

4 pages

Appendix V

Bio-Impedance FDM-Modelling Inside Heart for Application in Implanted Devices

Rauno Gordon, Alar Kuusik

Department of Electronics, TTU, Ehitajate tee 5
19086 Tallinn, Estonia, E-mail: rauno@elin.ttu.ee

Electrocardiology 2004
Proceedings of the 31st International Congress on Electrocardiology (ICE 2004) Kyoto, Japan

4 pages

Appendix VI

A Virtual System for Simultaneous Multi-frequency Measurement of Electrical Bioimpedance

R. Gordon*, R. Land*, M. Min**, T. Parve*, R. Salo***
*Department of Electronics, Tallinn University of Technology, Estonia
**Smartimplant Ltd., Tallinn, Estonia
***Basic Research Department, Guidant Corporation, St. Paul, Minnesota, USA

International Journal of Bioelectromagnetism
Vol. 7, No. 1, 2005

4 pages

Appendix VII

Accuracy of numerical methods in solving static and quasistatic electric fields

Rauno Gordon*, Tuukka Arola**, Katrina Wendel**, Outi Ryynanen** and Jari Hyttinen**
* Institute of Electronics, Tallinn University of Technology, Ehitajate tee 5, 19086 Tallinn, Estonia; rauno@elin.ttu.ee
** Ragnar Granit Institute, Tampere University of Technology, Biokatu 6, P.O. Box 692, FIN-33101 Tampere, Finland; tuukka.arola@tut.fi

Proceedings of Estonian Acadademy of Sciences, Engineering
2006, 12, 3-2, 262283

20 pages